GENETICS, 2025, 230(3), iyaf091
https://doi.org/10.1093/genetics/iyaf091
Advance Access Publication Date: 14 May 2025
Investigation

Conflicting Kinesin-14s in a single chromosomal drive haplotype

Meghan J. Brady,[1] Anjali Gupta ,[2] Jonathan I. Gent ,[3] Kyle W. Swentowsky,[4] Robert L. Unckless ,[5] R. Kelly Dawe [1,3,*]

[1]Department of Genetics, The University of Georgia, Athens, GA 30602, USA
[2]Department of Ecology and Evolutionary Biology, The University of Kansas, Lawrence, KS 66045, USA
[3]Department of Plant Biology, The University of Georgia, Athens, GA 30602, USA
[4]Cold Spring Harbor Laboratory, Cold Spring Harbor, NY 11724, USA
[5]Department of Molecular Biosciences, The University of Kansas, Lawrence, KS 66045, USA

*Corresponding author: Department of Genetics, The University of Georgia, B414A Davison Life Sciences, Athens, GA 30602, USA. Email: kdawe@uga.edu

In maize, there are 2 meiotic drive systems that target large heterochromatic knobs composed of tandem repeats known as knob180 and TR-1. The first meiotic drive haplotype, abnormal chromosome 10 (Ab10) confers strong meiotic drive (~75% transmission as a heterozygote) and encodes 2 kinesins: KINDR, which associates with knob180 repeats, and TRKIN, which associates with TR-1 repeats. Prior data show that meiotic drive is conferred primarily by the KINDR/knob180 system while the TRKIN/TR-1 system seems to have little or no role, making it unclear why *Trkin* has been maintained in Ab10 haplotypes. The second meiotic drive haplotype, K10L2, confers a low level of meiotic drive (~51–52%) and only encodes the TRKIN/TR-1 system. Here, we used long-read sequencing to assemble the K10L2 haplotype and showed that it has strong homology to an internal portion of the Ab10 haplotype. We also carried out CRISPR mutagenesis to test the role of *Trkin* on Ab10 and K10L2. The data indicate that the *Trkin* gene on Ab10 does not improve drive or fitness but instead has a weak deleterious effect when paired with a normal chromosome 10. The deleterious effect is more severe when Ab10 is paired with K10L2: in this context, functional *Trkin* on either chromosome nearly abolishes Ab10 drive. Mathematical modeling based on the empirical data suggests that *Trkin* is unlikely to persist on Ab10. We conclude that *Trkin* either confers an advantage to Ab10 in untested circumstances or that it is in the process of being purged from the Ab10 population.

Keywords: meiotic drive; neocentromere; heterochromatin; tandem repeats; chromosome segregation; kinesin; genomic conflict

Introduction

Selfish genetic elements are features of the genome that increase their own representation in the next generation despite conferring no fitness advantage (Burt and Trivers 2008). Meiotic drivers, 1 class of selfish genetic element, gain their advantage by altering meiosis so that they are transmitted to more than 50% of the gametes (Lindholm *et al.* 2016). Examples of meiotic drive that operate at the level of meiosis are centromere drive, where larger centromeres are preferentially transmitted over smaller centromeres, the segregation of some B chromosomes and the maize abnormal chromosome 10 (Ab10) haplotype (Fishman and Kelly 2015; Lampson and Black 2017; Clark and Akera 2021; Dawe 2022). There are also many other examples of drivers that exhibit preferential transmission by altering the viability of gametes after meiosis is complete (Lindholm *et al.* 2016). Meiotic drive has been implicated in critical evolutionary processes such as speciation, recombination, and genome size evolution (Haig and Grafen 1991; Plačková *et al.* 2024; Searle and Pardo-Manuel de Villena 2024). Ab10 is of particular interest as it has had a significant impact on shaping the evolution of maize, one of the most economically important crops (Buckler *et al.* 1999).

As much as >15% of the maize genome is composed of tandem repeat arrays (Hufford *et al.* 2021). One form of tandem repeat is referred to as knobs, which come in 2 different sequence classes, knob180 and TR-1. The Ab10 meiotic drive haplotype contains long arrays of both knob repeats as well as 2 kinesin protein-encoding genes: *Kindr* and *Trkin* (Fig. 1a). KINDR associates with knob180 knobs, and TRKIN associates with TR-1 knobs. Both KINDR and TRKIN are members of the Kinesin-14 family that moves cargo toward the minus ends of microtubules. They bind to their respective knobs and pull them ahead of the centromeres during meiotic anaphase to cause their preferential transmission to the egg cell during female meiosis, resulting in ~75% meiotic drive (Dawe 2022) (Fig. 1b). Knobs throughout the genome are also preferentially transmitted when Ab10 is present. Both knob180 and TR-1 are abundant across the *Zea* genus and in *Tripsacum dactyloides* suggesting that Ab10 may have originated deep in the evolutionary history of the grass family (Buckler *et al.* 1999; Swentowsky *et al.* 2020). The KINDR/knob180 system is primarily responsible for the preferential transmission of Ab10 while the TRKIN/TR-1 system contributes little, if at all (Kanizay *et al.* 2013; Dawe *et al.* 2018). Nevertheless, *Trkin* is present on multiple Ab10 haplotypes in both teosinte and maize suggesting it may have been maintained via selection over the ~8,700 years since their divergence (Piperno *et al.* 2009; Higgins *et al.* 2018; Swentowsky *et al.* 2020).

Received on 04 February 2025; accepted on 29 April 2025

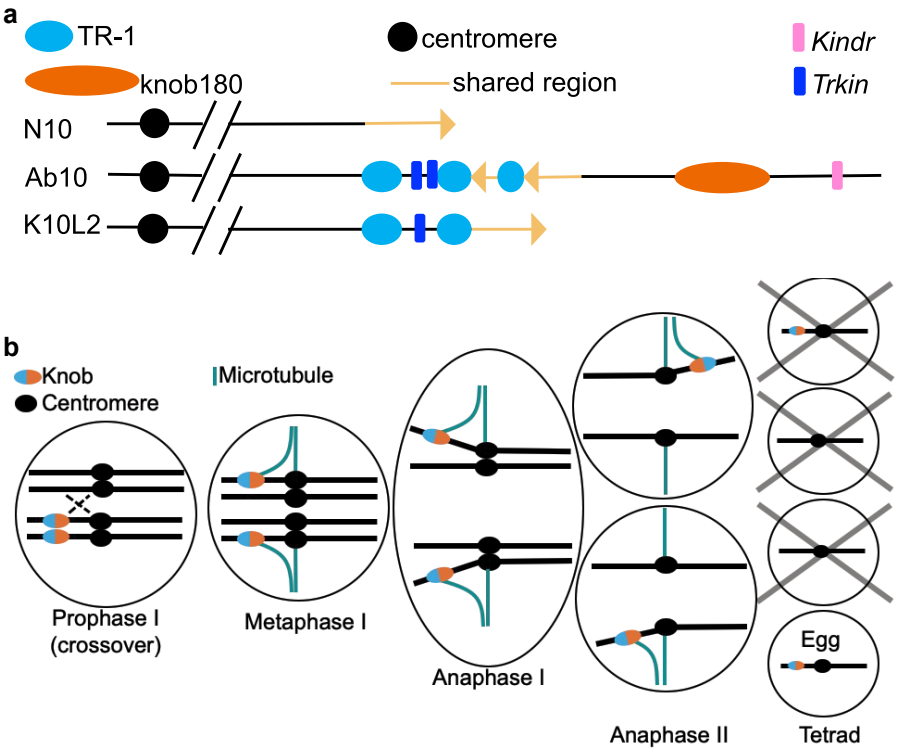

Fig. 1. Diagram of maize chromosome 10 haplotypes. a) Diagram of the structure of 3 chromosome 10 haplotypes. b) Model of Ab10 meiotic drive. For Ab10 drive to occur during female meiosis, the plant must be heterozygous for Ab10. Then, recombination must occur between the centromere and the edge of the Ab10 haplotype. During metaphase, TRKIN associates with TR-1 knobs and KINDR associates with knob180 knobs. Both Kinesin-14 proteins then drag the knobs ahead of the centromere during anaphase I and II causing their segregation to the top and bottom cells of the meiotic tetrad. Since only the bottom-most cell becomes the egg cell, Ab10 is overrepresented in progeny (Dawe *et al.* 2018; Swentowsky *et al.* 2020).

K10L2 is a structurally and functionally distinct variant of chromosome 10 that expresses TRKIN during meiosis and activates neocentromeres at TR-1 repeats (Kanizay *et al.* 2013) (Fig. 1). K10L2 demonstrates weak (51–52%) but statistically significant meiotic drive (Kanizay *et al.* 2013). Additionally, it has been identified in at least 12 disparate maize landrace populations suggesting it may be an important part of the Ab10 system (Kanizay *et al.* 2013). This level of drive should be sufficient to cause K10L2 to rapidly spread through a population as long as it is not associated with negative fitness consequences (Hartl 1970). K10L2 is also a very effective competitor against Ab10. When Ab10 is paired with K10L2, Ab10 drive is almost completely suppressed (Kanizay *et al.* 2013). It has been speculated that both the drive of K10L2 and the suppressive effect of K10L2 on Ab10 are mediated by the TRKIN/TR-1 system (Swentowsky *et al.* 2020).

The fitness costs commonly imposed on the genome by selfish genetic elements select for suppressors throughout the genome (Price *et al.* 2020). In the Ab10 system, both K10L2 and normal chromosome 10 (N10) represent disadvantaged loci. K10L2 can be thought of as both a disadvantaged locus carrying a highly effective suppressor when interacting with Ab10 and an independent driver when interacting with N10. The evolution of suppressors by co-opting the machinery of drive has been observed before (Price *et al.* 2020). For example, the *wtf* genes in *Schizosaccharomyces pombe* represent a toxin-antidote system. There are *wtf* loci carrying only the antidote that behave as suppressors to intact *wtf* loci (Bravo Núñez *et al.* 2018). If the Ab10 drive system followed the same model, we would expect that the TRKIN/TR-1 system (i.e. a suppressor) would appear only on K10L2 or N10. How or why *Trkin* persists on Ab10 while conferring little apparent benefit in terms of drive, and likely contributing to the suppression of drive when paired with K10L2, is unclear.

Two hypotheses have been proposed to resolve the conundrum of the TRKIN/TR-1 drive system on Ab10, each suggesting that *Trkin* improves the fitness of Ab10. The first is that *Trkin* may increase the transmission advantage of Ab10, and the second is that *Trkin* may reduce the negative fitness effects associated with Ab10 (Swentowsky *et al.* 2020). In previous work, the favored hypothesis was that *Trkin* reduces meiotic errors caused by the rapid movement of knobs during meiotic anaphase (Swentowsky *et al.* 2020). In this study, we set out to determine what effect *Trkin* has on Ab10 that may help to explain its persistence. We assembled the K10L2 haplotype and compared it to Ab10, then conducted drive and fitness assays of Ab10 and K10L2 haplotypes carrying *trkin* null alleles. Finally, we used mathematical modeling to better understand the predicted population dynamics of Ab10 haplotypes that carry *Trkin*.

Results

Assembly of K10L2 and Ab10

We began by generating a new assembly of Ab10 using PacBio HiFi sequencing. The Ab10 haplotype has been challenging to accurately assemble due to the prevalence of multiple repetitive arrays. The previous assembly of B73-Ab10 v1 was conducted with PacBio CLR data (single long reads) that have a higher error rate (Hon *et al.* 2020; Liu *et al.* 2020). To assess the quality and fidelity of the new assembly, we compared sequence homology between B73-Ab10 v1 (Liu *et al.* 2020) and the new assembly, B73-Ab10 v2. We found strong homology between the assemblies and the same

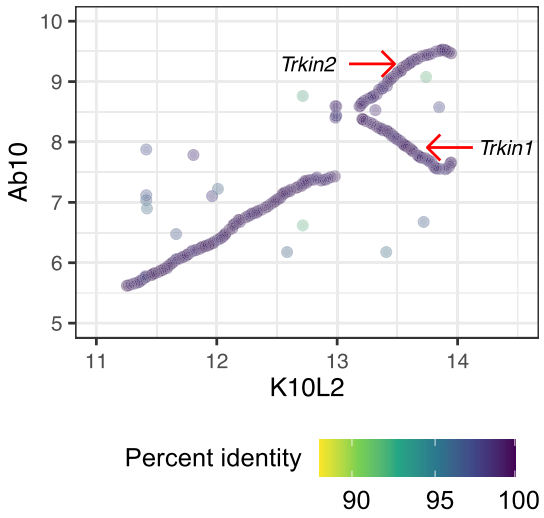

Fig. 2. Sequence comparison of *Trkin* bearing region on Ab10 and K10L2. Each dot marks the start of a maximal unique match of at least 300 bp between the Ab10 and K10L2 haplotypes. Coordinates start at the *colored1* gene and are shown in Mb. The color of each dot represents the percent identity of that match. All large knob arrays were removed for clarity. Both Ab10 *Trkin* genes are marked.

relationship to N10 as previously reported (Supplementary Figs. 1 and 2b). In both assemblies, the Ab10 haplotype is located at the end of the long arm of chromosome 10 as expected (Liu *et al.* 2020; Dawe 2022). The total size is unknown because of N-gaps predominantly within tandem repeat arrays, but we estimate the Ab10 haplotype contains about 77 Mb of sequence, with the proximal edge traditionally defined as the *colored1* (*r1*) gene (a linked marker used to track Ab10 in crosses). Segments of N10 are embedded within the Ab10 haplotype in the form of 2 large inversions of 4.8 and 9.5 Mb, which we refer to collectively as the shared region (Fig. 1a; Supplementary Fig. 2b). These are slightly longer than reported in B73-Ab10 v1 assembly (Liu *et al.* 2020). There are 3 TR-1 knobs (assembled length = 8.7 Mb collectively) and a very large knob180 knob (partially assembled length = 8.5 Mb). Both the TR-1 and knob180 knobs assembled lengths are slightly lower than in the B73-Ab10 v1 assembly (Liu *et al.* 2020). We used data from terminal deletion lines of Ab10 (Brady *et al.* 2024), to estimate that the Ab10 knob180 knob is ~30.67 Mb long, suggesting that it is only 28% assembled. There is also at least ~22 Mb of sequence that is unique to Ab10. The 1.8-Mb region between the first 2 TR-1 knobs includes 2 copies of *Trkin* (Fig. 2). The region to the right of the large knob180 knob contains an array of *Kindr* genes. Interestingly, there was a marked reduction in percent identity between the 2 assemblies over large tandem arrays like *Kindr* (Supplementary Fig. 1). This is likely due to the increased accuracy of PacBio HiFi reads (Hon *et al.* 2020). In fact, we identified 10 copies of *Kindr* in B73-Ab10 v2 instead of 9 as previously reported in B73-Ab10 v1 (Liu *et al.* 2020) (Supplementary Fig. 2d).

We next assembled the K10L2 haplotype. We found a distinct structure with 2 large TR-1 knobs (15.5 Mb collectively) and a 2.7-Mb nonshared region with a single copy of *Trkin* between them (Fig. 1a; nonshared means a lack of homology to N10). Otherwise, we found no large inversions or other rearrangements relative to N10 (Supplementary Fig. 2a). Additionally, we found no tandemly repeated genes (i.e. *Kindr* array), which are common on Ab10 (Supplementary Fig. 2) (Dawe *et al.* 2018). Sequence comparisons revealed the region between the 2 TR-1 knobs on K10L2 has strong homology to the *Trkin* bearing region on Ab10. However, unlike K10L2, Ab10 contains an inverted duplication with a second copy of *Trkin* (Fig. 2; Supplementary Fig. 2) (Swentowsky *et al.* 2020). The second copy of *Trkin* on Ab10 was previously thought to be a pseudogene and was referred to as Ab10 *pseudo-Trkin1* (Swentowsky *et al.* 2020). During this study, we found that the coding sequence (CDS) of *pseudo-Trkin1* was misinterpreted and that it instead encodes a full-length open reading frame. Accordingly, we have renamed *pseudo-Trkin1* to *Trkin2* (Fig. 3).

Genomic sequence of 3 *Trkin* genes reveals near identical intronic transposons

We annotated the B73-Ab10 v2 and K10L2 assemblies using BRAKER v3.0.8 (Gabriel *et al.* 2024), which was not available at the time of the B73-Ab10 v1 assembly (Liu *et al.* 2020). This allowed us to identify the full unbiased structure of each independent copy of *Trkin* on both Ab10 and K10L2. In line with the strong homology between the Ab10 haplotype and K10L2, inspection of the *Trkin* genomic sequence revealed a similar atypical structure between all 3 *Trkin* genes. Ab10 *Trkin1* spans 113 kb and Ab10 *Trkin2* spans 99 kb, while K10L2 *Trkin* spans 89 kb. The size differences are due to the presence of 9 transposable elements in the introns of Ab10 *Trkin1* and 2 transposable elements in the introns of Ab10 *Trkin2* relative to K10L2 *Trkin*. The transposable elements in Ab10 *Trkin1* and Ab10 *Trkin2* are not shared suggesting duplication and divergence after separation from the K10L2 *Trkin*. Notably, Ab10 *Trkin1* and *Trkin2* carry all the transposable elements that are present in K10L2 *Trkin* (Fig. 4). These data suggest that K10L2 *Trkin* is ancestral to the Ab10 *Trkin* genes.

Comparison of 3 *Trkin* genes reveals very few differences

Interrogation of the *Trkin* CDSs revealed that all 3 *Trkin* genes are remarkably similar with little evidence of functional divergence (Fig. 3a). Ab10 *Trkin1* contains 6 point mutations relative to K10L2 *Trkin*. Five of these produce nonsynonymous amino acid substitutions (one in an unstructured region, one in the coiled coil domain, and three in the motor domain). Ab10 *Trkin2* contains only 4 point mutations relative to K10L2 *Trkin*, of which 3 cause nonsynonymous amino acid substitutions (one in an unstructured region and two in the motor domain). Ab10 *Trkin1* and *Trkin2* differ by only 2 point mutations resulting in nonsynonymous amino acid substitutions (one in the coiled coil domain and one in the motor domain) (Fig. 3a). These data suggest that the differing effects of *Trkin* between Ab10 and K10L2, if any exist, are not due to differences in the encoded proteins.

We generated a neighbor-joining tree using all 3 TRKIN proteins and their closest maize homolog DV1 (Higgins *et al.* 2016), with the *Drosophila* Kinesin-14 NCD (McDonald *et al.* 1990) as an outgroup. We found that Ab10 TRKIN1 and TRKIN2 are more similar to each other than K10L2 TRKIN (Fig. 3b). This relationship suggests that the Ab10 *Trkin* genes duplicated after they diverged from K10L2 *Trkin*, in agreement with the inferences from the TE profile (Fig. 4).

Gene orthology between the 3 chromosome 10 haplotypes finds high agreement in the *Trkin* bearing region and unexpected orthologs in the Ab10 nonshared region

We next investigated gene orthology between all 3 assembled structural variants of chromosome 10 (Fig. 5). We define the

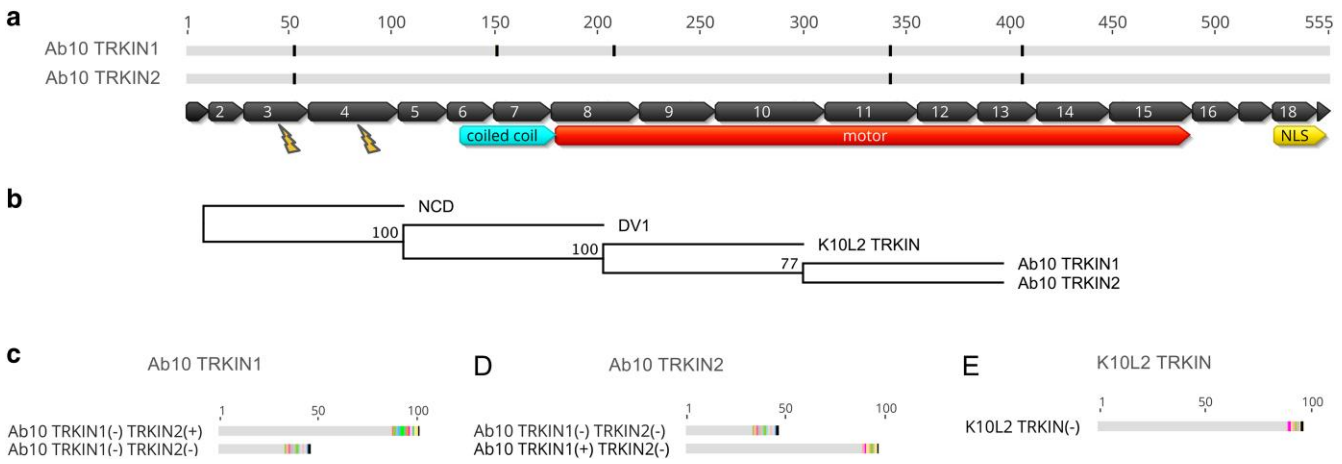

Fig. 3. Comparison of TRKIN proteins and mutants. a) Alignment of TRKIN proteins. Gray indicates sequence that is identical to the K10L2 TRKIN; black indicates sequence that is different from the K10L2 TRKIN. Exons are marked by numbered black boxes. Protein domains are marked by colored boxes (Swentowsky *et al.* 2020). Lightning bolts indicate exons that Cas9 was targeted to. b) Neighbor-joining consensus tree of the motor domains from all 3 TRKIN proteins, the closely related DV1 protein (Higgins *et al.* 2016) and *Drosophila* Kinesin-14 NCD (McDonald *et al.* 1990) using Jukes–Cantor model and 1,000 bootstraps. Numbers at nodes indicate the number of replicate trees supporting that node. c) Predicted truncated protein sequences of TRKIN1 mutants. d) Predicted truncated protein sequences of TRKIN2 mutants. e) Predicted truncated protein sequence of the K10L2 TRKIN mutant. In c)–e), the scale is the same as in a), and the colored bars represent out-of-frame amino acids. NLS, nuclear localization signal.

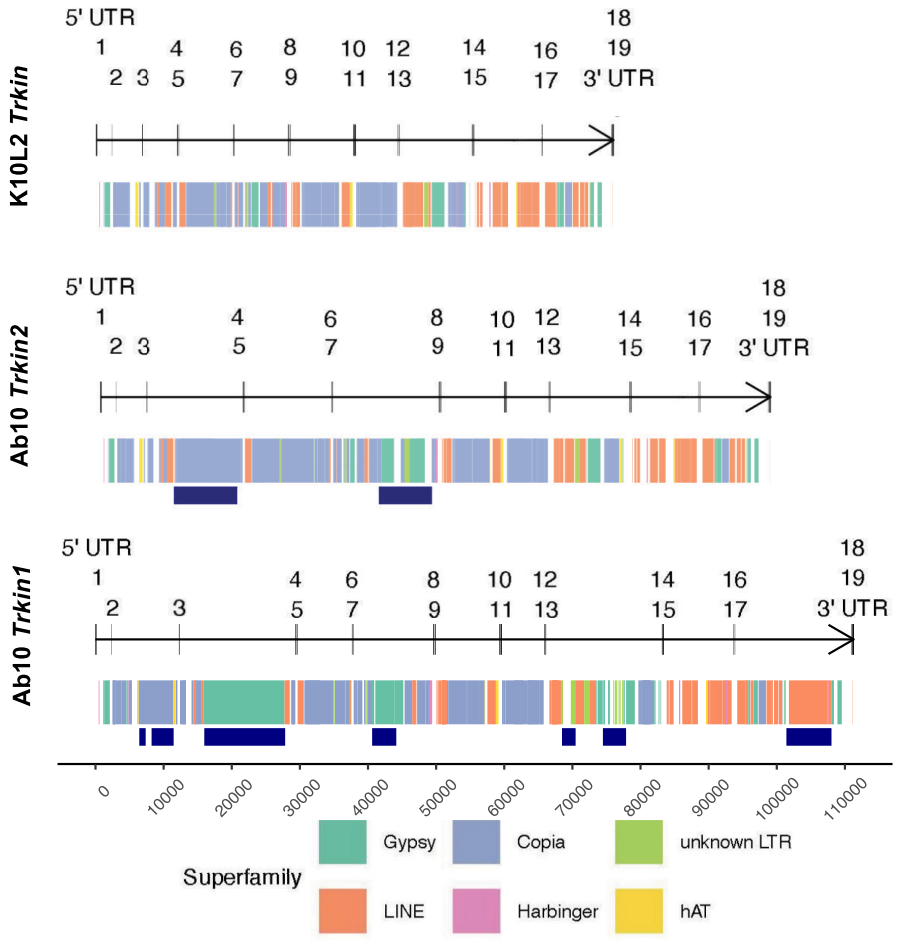

Fig. 4. Comparison of transposable element composition between all genes. Genomic sequences for all 3 *Trkin* alleles. Numbered vertical long black lines indicate *Trkin* exons. Annotated transposable elements are colored by their superfamily. Navy bars below the annotated transposable element blocks indicate insertions unique to that *Trkin* allele.

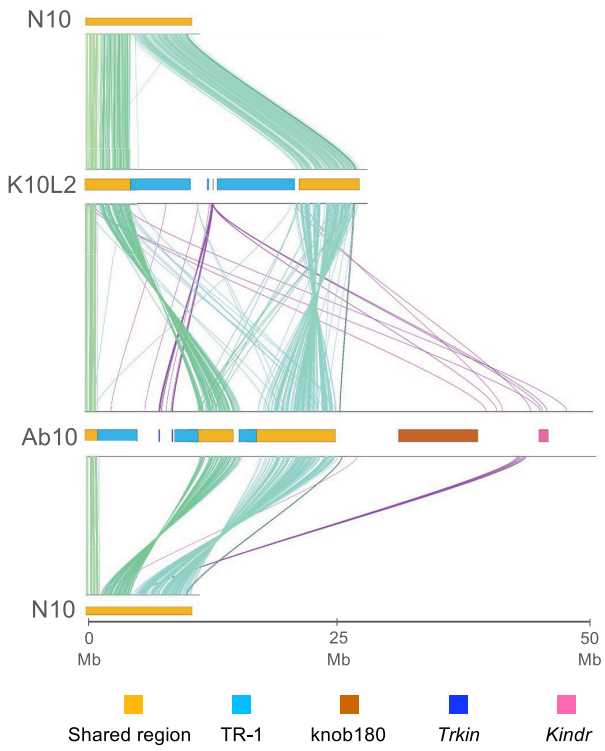

Fig. 5. Gene ortholog comparisons among chromosome 10 haplotypes. Each line represents a gene ortholog pair as determined by OrthoFinder (Emms and Kelly 2019). Shades of green represent gene ortholog pairs in different parts of the shared region (the first uninverted region, the first and second inversions, and the second uninverted region). Purple represents gene ortholog pairs outside of the shared region. Relevant regions of each haplotype are marked by colored bars. K10L2 and Ab10 refer to the assemblies generated in this work. N10 refers to the B73 v5 assembly (Hufford *et al.* 2021).

shared regions of Ab10 and K10L2 as the regions with significant homology to N10 and nonshared regions as those without significant homology to N10 (Supplementary Fig. 2; Fig. 5). There are 12 gene ortholog pairs in the Ab10 *Trkin* region and K10L2 *Trkin* region representing 44% (12/27) of annotated genes in this region on K10L2 and 66% (12/18) of the annotated genes in this region of Ab10 (Fig. 5; Supplementary Tables 1–3). There are also unexpected gene ortholog pairs between the shared regions of N10 and K10L2 and the nonshared region of Ab10 (Fig. 5; Supplementary Tables 4 and 5). Among the newly identified genes are 9 partial copies of a gene homologous to *nrpd2/e2*, which functions in RNA-dependent DNA methylation (Fig. 5; Supplementary Fig. 3). This is of particular interest as it has been hypothesized that RNA-dependent DNA methylation may be involved in the antagonistic dynamics between Ab10 and the host genome (Dawe *et al.* 2018).

Ab10 nonshared region annotations are enriched for RNA-dependent DNA methylation GO terms

We went on to perform a functional annotation of the Ab10 and K10L2 haplotypes using EnTAP (Supplementary Tables 1 and 2) (Hart *et al.* 2020; Gabriel *et al.* 2024). Incorporating all gene annotations, Ab10 is significantly enriched for Gene Ontology (GO) terms related to RNA-dependent DNA methylation due to the high copy number of *nrpd2/e2* (Supplementary Fig. 4). We also reduced all known tandemly duplicated genes to a single copy and reran the analysis. Under these conditions, Ab10 is enriched for GO terms related to meiotic organization and microtubule-based movement, in agreement with our understanding of the mechanism of drive (Supplementary Fig. 5) (Dawe 2022). In contrast, the K10L2 haplotype was enriched for general reproductive processes, ATP hydrolysis, and several other miscellaneous GO terms (Supplementary Fig. 6).

Trkin expression in K10L2 and Ab10 lines

The *Trkin* copy number difference between Ab10 and K10L2 led us to wonder if they may also have expression level differences. We obtained RNA-sequencing (RNA-seq) data from Ab10 and K10L2 anthers and mapped it to the B73-Ab10 v1 assembly (Liu *et al.* 2020; Swentowsky *et al.* 2020). The data revealed no consistent difference in *Trkin* expression between Ab10 bearing 2 copies and K10L2 bearing 1 copy of *Trkin* (Supplementary Fig. 7).

We also assessed the relative expression of *Trkin1* and *Trkin2* on Ab10. Analysis of RNA-seq data from 10 tissues from a homozygous Ab10 line (Liu *et al.* 2020) indicated that the expression of *Trkin2* is ~93% lower on average than *Trkin1* ($t = 6.5$, $df = 41.4$, $P = 6e^{-08}$) (Supplementary Fig. 8).

Generation of *trkin* knockout mutants on K10L2 and Ab10

To knock out the *Trkin* gene on both Ab10 and K10L2, we designed a CRISPR construct with 3 guide RNAs targeting exons 3 and 4 (Fig. 3). When we initiated the CRISPR mutagenesis, we were under the impression that Ab10 *Trkin2* was a pseudogene and did not assay it for mutations; the primers were designed to be specific to Ab10 *Trkin1* (Supplementary Table 6) (Swentowsky *et al.* 2020). Later, when we determined that Ab10 *Trkin2* is likely functional, we developed primers specific to Ab10 *Trkin2* and found that it was mutated in the line we were using as a positive control in our field crosses (see below). We isolated the following mutations: K10L2 *trkin*(–), Ab10 *Trkin1*(+) *trkin2*(–), Ab10 *trkin1*(–) *Trkin2*(+), and Ab10 *trkin1*(–) *trkin2*(–) (Fig. 3c–e).

Based on the strong correlation between *Trkin* and TR-1 neocentromere activity (Swentowsky *et al.* 2020), we expected *trkin* mutants to lack TRKIN protein and visible TR-1 neocentromeres at meiosis. In the K10L2 *trkin*(–) mutant plants, we could not detect TRKIN by immunostaining, whereas K10L2 *Trkin*(+) showed strong TRKIN staining (Fig. 6). In the Ab10 *trkin1*(–) *trkin2*(–) double mutant plants, we could not detect TRKIN by immunostaining and observed no TR-1 neocentromeres by FISH (Figs. 6 and 7), whereas Ab10 *Trkin1*(+) *trkin2*(–) showed strong TRKIN staining and TR-1 neocentromeres (Figs. 6 and 7). We did not observe TRKIN localization or TR-1 neocentromeres in plants of the Ab10 *trkin1*(–) *Trkin2*(+) genotype, which likely reflects the fact that *Trkin2* is expressed at very low levels (Supplementary Fig. 8).

The *Trkin* gene is required for K10L2 to suppress meiotic drive of Ab10

Prior work had established that when Ab10 is paired with K10L2, meiotic drive is strongly suppressed (Kanizay *et al.* 2013). We hypothesized that K10L2 *Trkin* may be responsible for this phenomenon. We found strong drive suppression when either Ab10 *Trkin1*(+) or K10L2 *Trkin*(+) was present and weaker suppression when only Ab10 *Trkin2*(+) was present (Fig. 8). In contrast, when *trkin* was completely knocked out on both Ab10 and K10L2, drive was fully restored to Ab10/N10 levels (Fig. 8; Supplementary Fig. 9). This demonstrates that *Trkin* is necessary for K10L2 to compete with Ab10.

These data suggest that the TRKIN encoded on Ab10 can bind to the TR-1 knob on K10L2 to suppress Ab10 drive, in other words, that Ab10 encodes its own context-dependent suppressor. Ab10

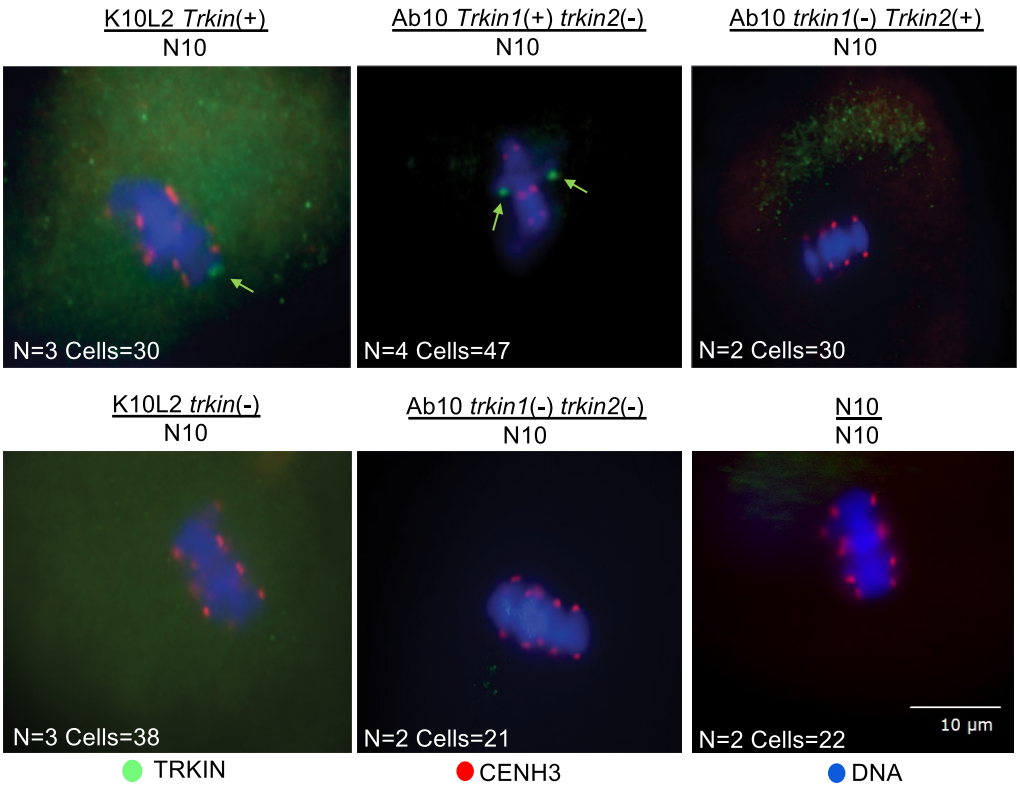

Fig. 6. TRKIN immunofluorescence in various *trkin* genotypes. All images show metaphase I except for Ab10 *Trkin1*(+) *trkin2*(–), which is metaphase II. *N* indicates the number of individual plants observed; Cells indicates the number of appropriately staged cells observed. Arrows mark TRKIN staining.

with active *Trkin1* should lose most of its drive whenever it encounters K10L2, variants of K10L2 that lack *Trkin*, or any other chromosome 10 with a large TR-1 knob. It remains theoretically possible that TRKIN preferentially localizes on TR-1 repeats of Ab10 or K10L2 due to unidentified divergence between these TR-1 repeats; however, we consider this unlikely because prior work indicates that neocentromeres are observed on all TR-1 knobs in lines carrying either haplotype (Hiatt *et al.* 2002; Hiatt and Dawe 2003).

Field and greenhouse experiments reveal no positive fitness effect of *Trkin*

Given the persistence of *Trkin* on the Ab10 haplotype, it seemed possible that it provides some benefit either through increased drive or reduced fitness effects (Buckler *et al.* 1999; Swentowsky *et al.* 2020). We tested this hypothesis by crossing our Ab10 *trkin* mutant lines as heterozygotes [*R1*-Ab10 (edited *trkin* alleles)/ r1-N10] with pollen from *r1/r1* homozygous plants in a large, randomized field design. For these tests, we did not have a true wild-type Ab10 control (with 2 functional *Trkin* genes), so we compared lines with 1 functional copy of either *Trkin1* or *Trkin2* to double mutants that lacked both genes.

Drive was measured by counting kernels carrying the dominant *R1* allele, which makes the kernels purple (*r1/r1* is colorless). We found that Ab10 *trkin1*(–) *trkin2*(–) had significantly higher drive than both Ab10 single *trkin* mutants with a mean difference of 0.41% [*trkin1*(–) *Trkin2*(+)] and 0.96% [*Trkin1*(+) *trkin2*(–)] (Fig. 9a). These effect sizes are quite small and right at the edge of what our experiment had power to detect. We had 51.8% power to detect a 1% change in drive and 82.8% power to detect a 1.2% change in drive. These data indicate that *Trkin* does not function to increase Ab10 drive under the tested experimental conditions. Instead, *Trkin* appears to decrease drive.

It has previously been suggested that *Trkin* may improve Ab10 fitness by preventing anaphase segregation errors that might occur when centromeres and neocentromeres move in opposite directions on the spindle (Swentowsky *et al.* 2020). Such errors would be expected to cause increased numbers of aborted kernels. On the same ears used for testing drive, we found that Ab10 *Trkin1*(+) *trkin2*(–) had a significantly higher proportion of defective kernels than Ab10 *trkin1*(–) *Trkin2*(+) with a mean difference of 0.41%. However, Ab10 *trkin1*(–) *trkin2*(–) did not have a significantly different proportion of defective kernels than either single mutant (Fig. 9b). We had 13% power to detect a 0.4% change and 78.2% power to detect a 0.8% change in kernel abortion. We also tested the effect of *Trkin* on the total number of kernels and found no significant differences between any genotypes (Fig. 9c). We had 80% power to detect down to a 30 kernel (~8.54%) difference. These data indicate that *Trkin1* does not reduce kernel abortion or alter total kernel count.

It is well understood that Ab10 causes severe reductions in kernel count and weight when homozygous (Higgins *et al.* 2018). We hypothesized that *Trkin* may be ameliorating some of the deleterious fitness effects when Ab10 is homozygous. We created an F2 population segregating for Ab10 *Trkin1*(+) *trkin2*(–) and Ab10 *trkin1*(–) *trkin2*(–) and conducted greenhouse fitness experiments. We found no significant effects on plant height, average kernel weight, or competitiveness between Ab10 haplotypes (intra-Ab10 competition) with respect to *trkin* genotype (Supplementary Fig. 10). We had power to detect differences of

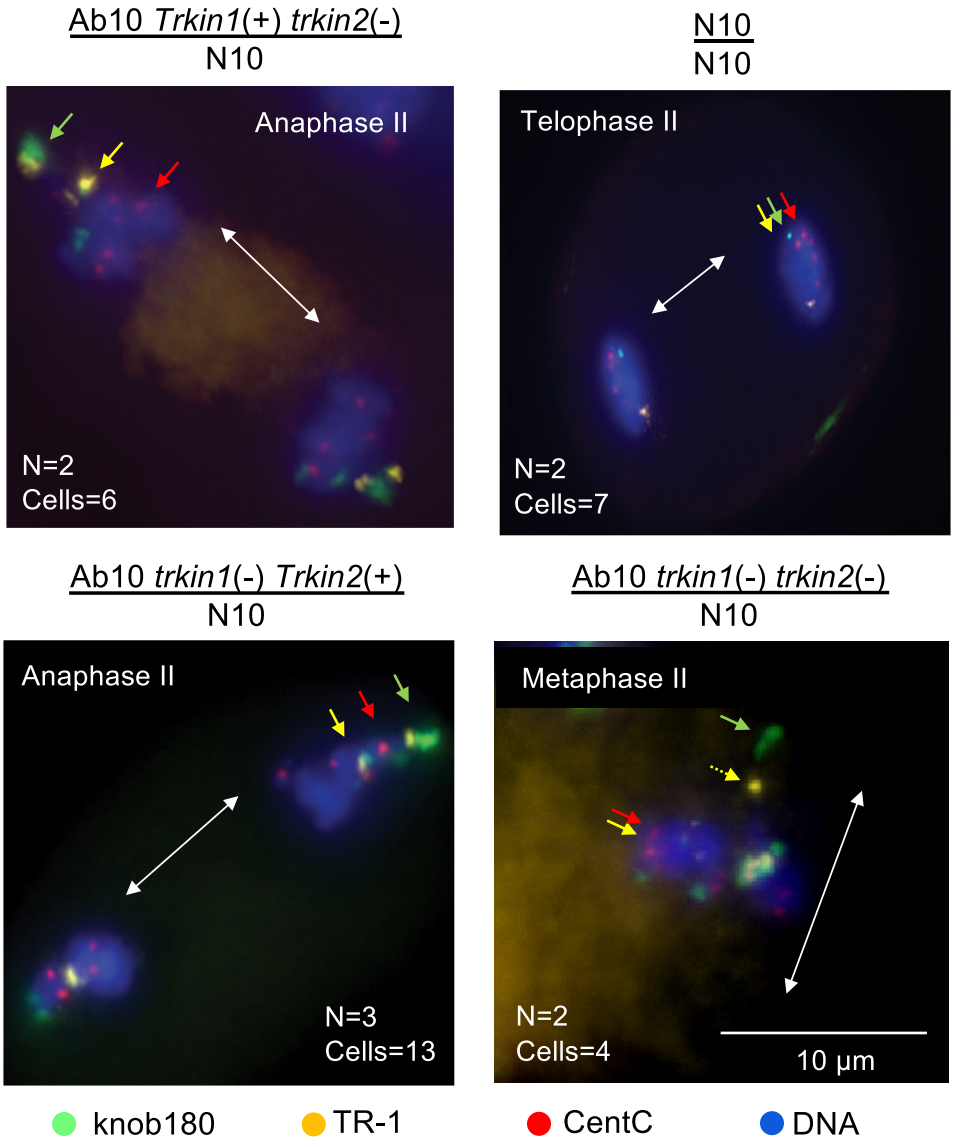

Fig. 7. FISH for neocentromere activity in various *trkin* genotypes. All plants were homozygous for their respective genotype. The cells are in differing stages of meiosis as indicated. The double-sided arrows indicate the spindle axis, showing which way the chromosomes were moving at the time of fixation. In the absence of TRKIN activity, TR-1 should be located behind the centromeres. The TR-1 knob that is off the metaphase plate in the lower right panel (dotted arrow) is being pulled by the large knob180 knob (this is likely Ab10 itself). *N* indicates the number of individual plants observed; Cells indicate the number of appropriately staged cells observed.

the following magnitudes: height = 52 cm (32% change), average kernel weight = 0.07 g (48% change), and intra-Ab10 competition = 21% change. Although, in this small study, we only could have detected large changes, the data indicate that *Trkin1* does not improve the fitness of Ab10 in the homozygous state.

The *Trkin1* gene does not reduce the frequency of meiotic errors in male meiosis

To test the effects of Ab10 *Trkin* on the accuracy of male meiosis, we screened Ab10 homozygous male meiocytes under the microscope for meiotic errors. Prior data demonstrated that homozygous Ab10 plants have reduced pollen viability (Higgins *et al.* 2018). We found no differences in meiotic errors between Ab10 *Trkin1*(+) *trkin2*(–), Ab10 *trkin1*(–) *Trkin2*(+), and Ab10 *trkin1*(–) *trkin2*(–) lines or N10 lines (Supplementary Fig. 11). We had 80% power to detect down to the following differences: tetrad micronuclei = 5%, tetrad microcyte = > 0%, dyad micronuclei = 36%, and total meiotic errors = 6%. These data provide further evidence that Ab10 *Trkin1* does not reduce the frequency of meiotic segregation errors that might occur when centromeres and neocentromeres move in opposite directions on the spindle (Swentowsky *et al.* 2020).

The *Trkin1* gene does not affect the degree of meiotic drive at an unlinked mixed knob

Trkin is known to activate neocentromeres throughout the genome (Dawe 2022). It seemed possible that *Trkin* behaved differently with other TR-1 knobs in the genome. To test the effect of *Trkin* on knobs elsewhere in the genome, we looked at its effect on the transmission of a large mixed knob on chromosome 4L marked by a GFP-encoding insertion that expresses in kernel endosperm (Li *et al.* 2013). We found no significant difference in segregation of the 4L knob between Ab10 with functional *Trkin1* or without functional *trkin*. We also found no difference in K10L2 *Trkin*(+) or

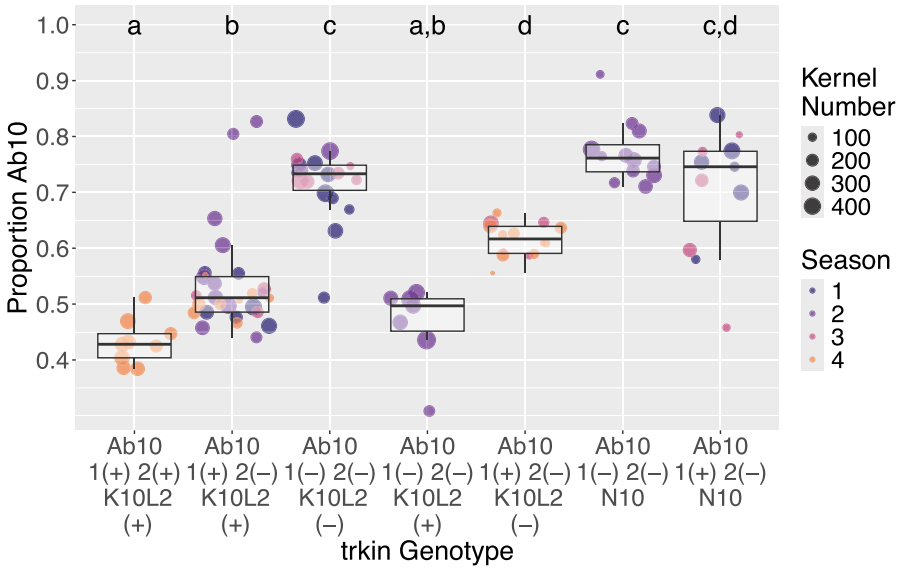

Fig. 8. Effect of *Trkin* on the meiotic drive of Ab10 when paired with K10L2. The plot shows meiotic drive as measured by the percentage of kernels carrying the *R1* allele linked to Ab10. All plants were grown in the greenhouse in Athens, GA, USA. Each dot represents an individual plant. Season refers to a group of plants grown at the same time. Seasons 1 and 2 were conducted in the same genetic background while seasons 3 and 4 were conducted in different genetic backgrounds. Seasons 1 and 2 of the Ab10 *trkin1*(–) *trkin2*(–) and *K10L2 trkin*(–) had *Cas9* segregating; refer to Supplementary Fig. 9 for details. The Wilcoxon signed-rank test was proportion Ab10 ~ *trkin* genotype. Genotypes with the same letter above them are not significantly different; genotypes with different letters above them are significantly different; refer to Supplementary Fig. 9 for specifics.

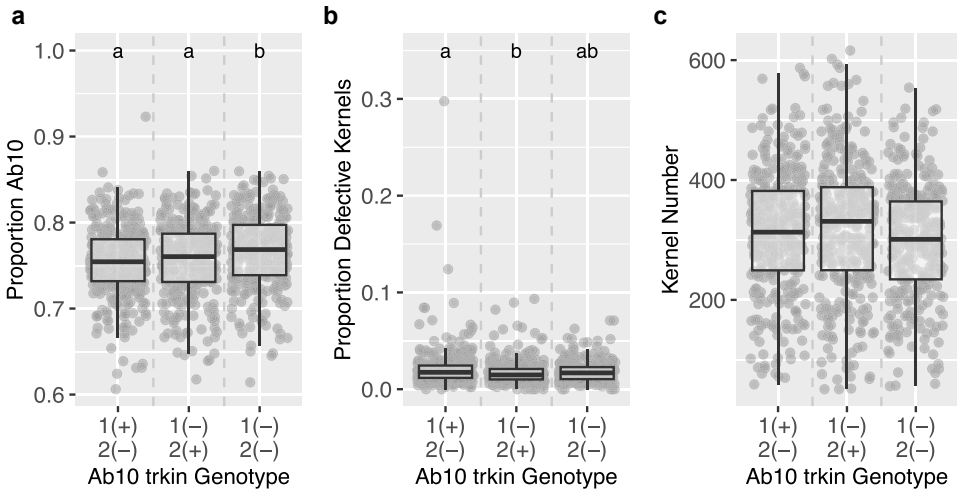

Fig. 9. Ab10 drive and plant fitness effects of *Trkin* in Ab10 heterozygotes. Plants were grown in randomized order in a field in Molokai Hawaii. a) Meiotic drive as measured by the percentage of kernels carrying the *R1* allele linked to Ab10. b) Proportion of defective kernels. c) Kernel number. Each dot represents an individual plant. Genotypes with the same letter above them are not significantly different; genotypes with different letters above them are significantly different.

trkin(–). We had 80% power to detect down to an 8% difference in segregation (Supplementary Fig. 12). Together, these data indicate that *Trkin* does not have an outsized effect on knobs elsewhere in the genome, just as it has little or no effect on Ab10.

Modeling suggests that Ab10 *Trkin*(+) is likely to be replaced by Ab10 *trkin*(–) in maize populations

The above evidence indicates that *Trkin* has a negative effect on Ab10 fitness. While it remains possible *Trkin* has some benefit we were unable to detect, we wanted to examine the population dynamics of *Trkin* in the long term using a modeling approach. We built on the prior Ab10 meiotic drive model (Hall and Dawe 2018) to include Ab10 *Trkin*(+), Ab10 *trkin*(–), K10L2, and N10, and examined Ab10 *Trkin*(+) dynamics in populations. Specifically, we asked 3 questions for a subset of parameters representative of the empirical system: (1) when and how often does Ab10 *Trkin*(+) outcompete Ab10 *trkin*(–) in a population, (2) is the evolution of Ab10 *Trkin*(+) likely to be dominated by natural selection or genetic drift, and (3) how long does it take for Ab10 *trkin*(–) to eventually replace Ab10 *Trkin*(+) in a population?

We began with simulations following a deterministic model (assuming discrete nonoverlapping generations, diploid organisms, and a single panmictic population of infinite size). We found that Ab10 *Trkin*(+) can never invade a population at equilibrium with Ab10 *trkin*(–) as long as there is selection against the *Trkin*(+) allele. This selection against the *Trkin*(+) allele is

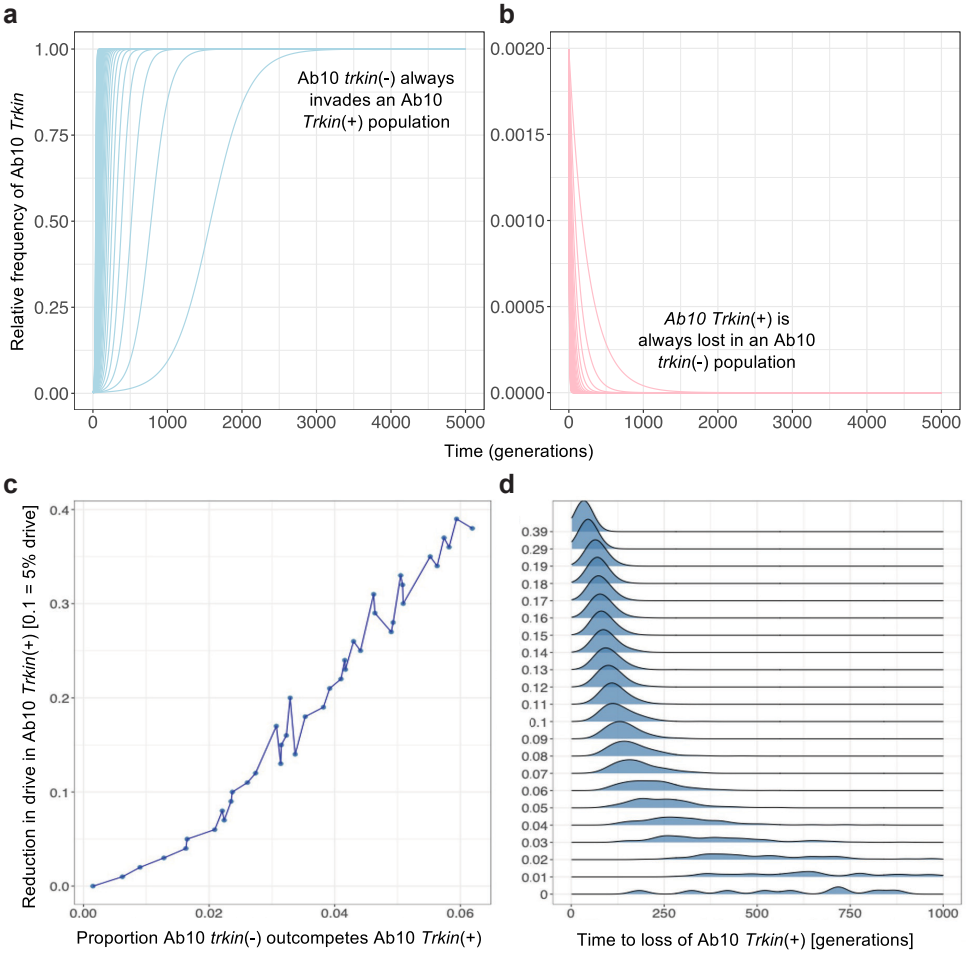

Fig. 10. Population dynamics of *Trkin* alleles in population genetic models. a, b). Deterministic simulations show that *trkin*(–) always replaces *Trkin*(+) regardless of the parameters employed. a) Ab10 *trkin*(–) always replaces Ab10 *Trkin*(+) when introduced into a population segregating for Ab10 *Trkin*(+) at 5% frequency with N10 and K10L2 also segregating. b) Ab10 *Trkin*(+) is always lost when introduced into a population segregating for Ab10 *trkin*(–) with N10 and K10L2. In both cases, the different lines show several different values for the amount that Ab10 drive is suppressed by *Trkin*(+) denoted by δ_1 in our model. c, d). How long can Ab10 *Trkin*(+) persist in a population being invaded by Ab10 *trkin*(–)? Simulations were run stochastically, modeling drift following a multinomial distribution, at an initial frequency of 6% for Ab10 *Trkin*(+) and K10L2 and $1/N_e$ for Ab10 *trkin*(–) using $N_e = 10{,}000$ and for $0 < \delta_1 < 0.4$. Each simulation was iterated 10,000 times. c) Proportion of realizations Ab10 *trkin*(–) successfully invades into the population and replaces Ab10 *Trkin*(+). The parameter on the *y*-axis is represented by δ_1 in the model. Note that these proportions are small since Ab10 *trkin*(–) was often lost due to drift. d) Density distribution for the number of generations Ab10 *Trkin*(+) can persist in a population upon invasion by Ab10 *trkin*(–). The parameter on the *y*-axis is represented by δ_1 in the model.

associated with the fact that it suppresses Ab10's ability to drive. Additionally, we found that Ab10 *trkin*(–) can always invade a population at equilibrium with Ab10 *Trkin*(+) (Fig. 10a and b). Thus, unless the Ab10 *Trkin*(+) allele has some hidden or context-dependent benefit, it should not invade or segregate in a population assuming a deterministic model.

Next, we considered the strength of selection against Ab10 *Trkin*(+), reasoning that if selection is weak enough, genetic drift might dominate natural selection in small populations. If so, genetic drift might explain the persistence of Ab10 *Trkin*(+). We calculated the selection coefficient against Ab10 *Trkin*(+) compared to Ab10 *trkin*(–) for various values of reduction in drive due to *Trkin*. Selection predominates over drift if $2 * N_e * s > 1$, where s is the selection coefficient and N_e is the effective population size (Hartl and Clark 2007). So, we calculated $2 * N_e * s$ for a range of reductions of drive and effective population sizes. There are almost no combinations of parameters where selection against Ab10 *Trkin*(+) would be dominated by genetic drift ($2 * N_e * s < 1$). In fact, the effective population size would need to be <100 and the reduction in drive close to 0 for genetic drift dynamics to dominate; neither of which is realistic. Therefore, we concluded that selection against Ab10 *Trkin*(+) is strong enough that drift cannot explain its persistence.

Although genetic drift is unlikely to prevent Ab10 *trkin*(–) from overtaking Ab10 *Trkin*(+) in a population, drift may influence how long the process takes. Given that we know both Ab10 *trkin*(–) and *Trkin*(+) segregated in wild ancestors, this suggests both have persisted for at least 8,700 generations (Piperno *et al.* 2009; Swentowsky *et al.* 2020). Therefore, we assessed whether, given estimated parameters, the Ab10 *trkin*(–) might still be in the process of replacing Ab10 *Trkin*(+). Thus, we extended our deterministic model to a stochastic model (choosing genotypes from a multinomial distribution to simulate genetic drift). We asked how long it takes for Ab10 *trkin*(–) to replace Ab10 *Trkin*(+) when Ab10 *Trkin*(+) starts at a frequency of 6% (based on Kato 1976; Kanizay *et al.* 2013) and Ab10 *trkin*(–) starts as a single copy. Ab10 *trkin*(–)

introduced as a single copy would often be lost due to drift in a stochastic model (Haldane 1927). Figure 10c shows that the more the Ab10 *Trkin*(+) allele reduces drive, the more likely Ab10 *trkin*(–) is to escape stochastic loss and replace Ab10 *Trkin*(+). However, in nature, Ab10 *trkin*(–) exists so it must have escaped stochastic loss at some point (Swentowsky *et al.* 2020). Figure 10d shows the distribution for time to loss of Ab10 *Trkin*(+), given a rare Ab10 *trkin*(–) allele introduced in an Ab10 *Trkin*(+) population at equilibrium for Ab10 *Trkin*(+), K10L2, and N10 where Ab10 *trkin*(–) escaped stochastic loss. The mean time for loss of Ab10 *Trkin*(+), or the time it takes for Ab10 *trkin*(–) to replace Ab10 *Trkin*(+), is <500 generations. This is true if the reduction in drive is more than ~0.01 (our empirical estimates suggest the value is more like 0.1) (Fig. 9a). Therefore, we conclude that Ab10 *trkin*(–) should replace Ab10 *Trkin*(+) in <500 generations for most parameter combinations resembling the empirical system.

The results presented above fail to explain the long-term persistence of Ab10 *Trkin*(+). They suggest that either Ab10 *trkin*(–) is very young (<500 generations) and is currently replacing Ab10 *Trkin*(+) or that Ab10 *Trkin*(+) confers some fitness advantage that we did not observe.

Discussion

Despite examples of *Trkin* being encoded in all 3 common Ab10 variants and K10L2 (Swentowsky *et al.* 2020) and the conservation of TR-1 repeats across *Zea* and its sister genus *Tripsacum*, our data provide no evidence that *Trkin* provides a selective advantage to Ab10. Instead, under the conditions we tested, Ab10 *Trkin* slightly reduces Ab10 drive and acts as an efficient suppressor of drive in the presence of K10L2. Since we only fully tested the function of Ab10 *Trkin1*, we cannot rule out the possibility that *Trkin1* has a positive fitness effect only in the presence of functional *Trkin2*. We can, however, confidently conclude that Ab10 *Trkin1* is sufficient to activate TR-1 neocentromeres and allow K10L2 to compete with Ab10 independently of *Trkin2*. Modeling suggests that, under our current understanding of the system, Ab10 *Trkin1*(+) *trkin2*(–) is unlikely to persist in the population when Ab10 *trkin1*(–) *trkin2*(–) is present. We propose 2 theories for the existence of *Trkin* on the Ab10 haplotype: an advantage either smaller than could be detected here or only apparent in untested circumstances, or that *Trkin* is in the process of being purged from the Ab10 population.

Our best estimate of *Trkin* prevalence in the Ab10 population places it at around 50% (Swentowsky *et al.* 2020). It is possible that Ab10 *trkin*(–) is a new development. Perhaps in the past, *Trkin* served a function that has been lost in the last ~500 years and is now slowly being purged from the population. It may be that *Trkin* provides benefits to Ab10 in teosinte, but not in maize. However, maize was domesticated from teosinte ~8,700 years ago (Piperno *et al.* 2009) which our models suggest would have been ample time for *Trkin* to have been purged from the population (Fig. 10b). To explain the continued presence of Ab10 *Trkin*(+) in maize, it would have to be reintroduced via gene flow from teosinte, which is plausible (Yang *et al.* 2023). It is also possible that gene conversion or illegitimate recombination between Ab10 and K10L2 continuously reintroduces *Trkin* to Ab10.

K10L2 is a relatively common variant of chromosome 10 (Kato 1976; Kanizay *et al.* 2013) and is known to function as a suppressor of Ab10 drive (Kanizay *et al.* 2013). Our data demonstrate that the *Trkin* gene is specifically responsible for the ability of K10L2 to suppress Ab10 drive. The evolution of a suppressor on the disadvantaged allele is common in drive systems (Price *et al.* 2020). However, it is unusual and apparently paradoxical (as far as we know, this is the first example) for a driving haplotype to encode its own, albeit context dependent, suppressor. The Ab10 and K10L2 drive systems are clearly complex and have had a major impact on the evolution of maize. Our data suggest that we do not yet understand the full range of contexts where Ab10 either has historically functioned or is currently functioning as a meiotic driver. Further studies of Ab10 and other chromosome 10 variants in teosinte may help provide new leads and help us better understand the functions of *Trkin* in natural Ab10 populations.

Methods

Assembly of K10L2

CI66 (PI 587148) seed was ordered from the Germplasm Resources Information Network in Ames, IA, USA, and grown in the University of Georgia (UGA) Botany greenhouse in Athens, GA, USA. Leaf tissue was sent to the Arizona Genomics Institute for DNA extraction using a CTAB method (Doyle and Doyle 1987). The sequencing library was constructed using SMRTbell Express Template Prep kit 3.0. The final library was size selected on a Blue Pippin (Sage Science) with 10- to 25-kb size selection. Sequencing was performed on a PacBio Revio system in CCS mode for 30 h. We filtered reads to a quality of 0.99 or greater and converted them to fastq format using BamTools v2.5.2 and BEDTools 2.30.0, respectively (Quinlan and Hall 2010; Barnett *et al.* 2011). We ran hifiasm v0.19.6 with post-joining disabled to assemble the raw reads into contigs (Cheng *et al.* 2021). We identified the K10L2 haplotype by using BLAST v 2.13.0 to identify the contig with homology to the *Trkin* cDNA sequence (Swentowsky *et al.* 2020). This contig also contained 2 large TR-1 knobs. Using the integrated genome viewers motif finder, we determined that the *Trkin* bearing contig ended in 7,674 bp of telomere sequence indicating it was fully assembled (Thorvaldsdóttir *et al.* 2013). The *Trkin* bearing contig had no homology to the *colored1* gene, which marks the beginning of the Ab10 haplotype. To ensure that all the chromosome 10 haplotypes were comparable, we manually merged the *colored1* gene bearing contig with the contig containing the otherwise complete K10L2 haplotype with an interceding 100-N gap using RagTag v2.1.0 (Alonge *et al.* 2022).

Assembly of B73-Ab10 v2

We chose to generate a new Ab10 assembly as there had been significant methodological advances since the generation of the first assembly (Liu *et al.* 2020). We used the same high molecular weight genomic DNA that was used in the B73-Ab10 v1 assembly (Liu *et al.* 2020). The sequencing library was constructed using SMRTbell Express Template Prep kit 2.0. The sequencing library was prepared for sequencing with the PacBio Sequel II Sequencing kit 2.0 for HiFi libraries and sequenced in CCS mode at the UGA Georgia Genomics and Bioinformatics Core facility. These data were integrated into the previously published assembly pipeline to produce the B73-Ab10 v2 assembly (Liu *et al.* 2020).

Comparison of the B73-Ab10 v1 and B73-Ab10 v2 haplotypes

B73-Ab10 v1 and B73-Ab10 v2 were compared using Mummer v4.0.0 with a minimum length (-m) of 300 and computing all matches not only unique ones (–maxmatch) (Marçais *et al.* 2018; Liu *et al.* 2020). Plots were generated using R v4.3.1.

Annotation of Ab10 and K10L2

The assemblies described above were annotated for repeats and masked using RepeatMasker v4.1.5 (Smit *et al.* 2015) in conjunction with the maize repeat library (https://github.com/oushujun/MTEC). For gene annotation, all available short-read mRNA sequencing from Ab10 (Liu *et al.* 2020) and K10L2 (Swentowsky *et al.* 2020) were used. These reads were then aligned to their respective genomes using HiSat2 v3n-20201216 (Kim *et al.* 2019). The resulting files were converted to a bam format and sorted using SAMtools v1.17 (Kim *et al.* 2019; Danecek *et al.* 2021). These alignments were used as expression evidence, and the Viridiplantae partition of OrthoDB was used as protein evidence in an annotation using BRAKER v3.0.8 (Kuznetsov *et al.* 2023; Gabriel *et al.* 2024). Trinity v2.15.1 and StringTie v2.2.1 were used to assemble a de novo and reference-guided transcriptome from the compiled RNA-seq data for Ab10 and K10L2, respectively (Haas *et al.* 2013; Pertea *et al.* 2015). These transcriptomes were combined and converted to a comprehensive transcriptome database using PASA v2.5.3 (Haas *et al.* 2003). The resulting comprehensive transcriptome database was used to polish and add UTRs to the BRAKER-derived gene annotation file in 3 rounds of PASA v2.5.3 (Haas *et al.* 2003). We found that the *Trkin* bearing region on Ab10 and K10L2 has an average percent identity of 98.5% for aligned regions (Fig. 2). However, the annotated genes were quite different. In order to improve the annotations, we used Liftoff v1.6.3 to reciprocally update the annotations in the *Trkin* bearing region on both haplotypes (Shumate and Salzberg 2021). We then extracted only genes that were included in the Liftoff annotation using BEDTools v2.31.0 and incorporated them (Quinlan and Hall 2010). Genes added in this way have names starting with gA in the K10L2 annotation and gK in the Ab10 annotation. We extracted the CDS and cDNA sequences for both haplotypes using AGAT v1.1.0 (Dainat 2020). Finally, we extracted and functionally annotated the final protein sets using EnTAP v1.0.0 with the nr, Refseq, and UniProt databases (O'Leary *et al.* 2016; Hart *et al.* 2020; Sayers *et al.* 2022; UniProt Consortium 2023).

Determination of Ab10 knob180 knob size

We obtained Illumina sequence reads for terminal deletions of Ab10 in the W23 inbred background that either did or did not contain the large knob180 knob on the distal most end (Brady *et al.* 2024). We quantified knob180 repeat abundance in raw Illumina short reads as described in Hufford *et al.* (2021). In brief, we used seqtk v1.2 (https://github.com/lh3/seqtk) to convert the read files to fasta format, used BLAST v2.2.26 to identify reads with homology to knob180, and BEDTools merge v2.30.0 to combine overlapping hits (Quinlan and Hall 2010; Camacho *et al.* 2023). Using a custom R script, we filtered to hits 30 bp or longer, summed the lengths of all hits, and divided that value by the average coverage of the library to obtain the Mb value of knob180 in each library. We then subtracted the value of the intact W23-Ab10 from the sample, which did not contain the large knob180 knob to obtain the estimated size of the knob180 knob on Ab10. We repeated this process for TR-1 and CentC as negative controls.

Comparison of sequence homology between Ab10 and K10L2

All possible pairwise comparisons of chromosome 10 haplotypes were made using Mummer v4.0.0 with a minimum length (-m) of 300 and computed all matches, not only unique ones (–maxmatch). Self-by-self comparisons were run using the –nosimplify flag (Marçais *et al.* 2018). Plots were generated using R v4.3.1.

To assess the completeness of the *nrpd2/e2* gene homologs, we extracted the CDSs of all annotated copies using AGAT v1.1.0 (Dainat 2020). We then aligned all copies to the *nrpd2/e2* CDS from the B73 v5 assembly using Geneious Prime v2022.0.2 Geneious algorithm (Zm00001eb068960) (Hufford *et al.* 2021).

Comparison of *Trkin* CDS

The newly annotated *Trkin* gene was identified by overlap with the BLAST v2.13.0 hits for *Trkin* cDNA (Swentowsky *et al.* 2020) against the newly assembled references (Camacho *et al.* 2023). The associated CDS was extracted from the CDS file for the respective genomes produced using AGAT v1.1.0 (Dainat 2020). The CDSs were aligned using the Geneious Prime v2022.0.2 Geneious algorithm (https://www.geneious.com). Protein domain locations were determined using NCBI conserved domain search, the cNLS mapper, and the MPI Bioinformatics toolkit (Kosugi *et al.* 2009; Gabler *et al.* 2020; Wang *et al.* 2023).

To better understand the relationship between the *Trkin* alleles, we chose to make a phylogenetic tree using the protein motor domain. TRKIN does not share sufficient homology with similar proteins to use its entire length (Swentowsky *et al.* 2020). We used NCBI conserved domain search (Wang *et al.* 2023) to identify the motor domain in all the *Trkin* alleles as well as *Drosophila melanogaster* Ncd (UniProt P20480) and *Zea mays Dv1* (B73 v5 annotation Zm00001eb069600). We selected *Z. mays Dv1* as it is the most closely related gene to *Trkin* (Swentowsky *et al.* 2020). We selected *D. melanogaster* Ncd to act as an outgroup. We used Geneious Prime v2022.0.2 to perform a MUSCLE alignment of all 4 motor domains and used the Geneious tree builder to create a neighbor-joining tree using the Jukes–Cantor model. We set *Ncd* as the outgroup and performed 10,000 bootstrap replicates. Numbers at nodes indicate the percentage of replicate trees supporting that node.

Comparison of gene orthologs

Gene orthology between the 3 variants of the chromosome 10 haplotype was compared as described previously (Brady *et al.* 2024). For the purposes of this analysis, the beginning of each haplotype was determined to be the location of the *colored1* gene. Plots were generated using R v4.3.1.

GO term enrichment analysis

We isolated the nonshared region, defined as those areas with no consistent synteny or homology to N10 as determined by the gene ortholog analysis and sequence comparisons, for both Ab10 and K10L2. These genes were tested against the remaining portions of the genome for GO term enrichment using topGO (Alexa and Rahnenfuhrer 2024). The Ab10 nonshared region contains several known duplicated genes that heavily influence the results. All known arrayed gene duplicates were collapsed down to a single copy. The 2 copies of *Trkin* were both included.

Expression of *Trkin*

We obtained RNA-seq data for Ab10 and K10L2 from Swentowsky *et al.* (2020). We trimmed reads using Trimmomatic v0.39 (Bolger *et al.* 2014) and aligned them to the Ab10 v1 reference (Liu *et al.* 2020) using HiSat2 (Kim *et al.* 2019) and processed the output using SAMtools v1.9 (Danecek *et al.* 2021). We used the R package featureCounts to determine the expression for each annotated

gene (Liao et al. 2014). We then calculated the transcripts per million (TPM) for Ab10 *Trkin1* and Ab10 *Trkin2* in all samples requiring a mapping quality of 20. We summed the TPM of Ab10 *Trkin1* and *Trkin2* for easy comparison between Ab10 and K10L2.

To assess the expression of Ab10 *Trkin1* and *Trkin2* separately, we assessed expression at the individual exon level. We obtained RNA-seq data for 10 tissues of the B73-Ab10 inbred (Liu et al. 2020). We aligned them to the Ab10 v2 reference generated here using HiSat2 (Kim et al. 2019). We filtered the alignments to a mapping quality of 20 and required no mismatches. We then used the R package featureCounts to determine the expression of each annotated exon (Liao et al. 2014). We then calculated the TPM for only the *Trkin* exons containing SNPs (7 and 8) in all samples (Fig. 3). We used a Welch's 2-sample t-test to determine statistical significance between the 2 alleles.

Construction and transformation of a plasmid expressing Cas9 and guide RNAs

A CRISPR plasmid expressing Cas9 and 3 guide RNAs targeting *Trkin* was constructed using a pTF101.1 binary plasmid (Paz et al. 2004) with similar components as previously used for gene editing in maize (Wang et al. 2021). In particular, it utilizes 1,991 bp of a maize polyubiquitin promoter and UTR region (GenBank: S94464.1) to drive expression of Cas9 from *Streptococcus pyogenes* flanked by an N-terminal SV40 NLS and a C-terminal VirD2 NLS and followed by a polyadenylation signal provided by a *nopaline synthase* (*NOS*) terminator sequence from *Agrobacterium tumefaciens*. The Cas9 DNA sequence was codon optimized for maize as described previously except that it did not include the potato ST-LS1 intron (Svitashev et al. 2015). The 3 guide RNAs were transcribed by 3 individual U6 promoters from maize and rice with 2 guide RNAs targeting *Trkin* exon 3 (GTCTGGAGGCCAATGAGCACG and GAAAGCTTTTGCGGCCTCTGG) and 1 targeting exon 4 (GCCTACACAAGTAAACAGAT). These target sequences were selected using CHOPCHOP v3 (Labun et al. 2019). Complete plasmid sequence and annotations are available at https://github.com/dawelab/TRKIN_Published.git. Gene synthesis and cloning were performed by GenScript (www.genscript.com), and transformation was performed by the Iowa State University Plant Transformation Facility.

Genotyping for *trkin* mutants

All DNA extractions were performed using a CTAB protocol (Clarke 2009). PCRs were performed using Promega GoTaq Green Master Mix (M7123). The Ab10 *trkin1* and K10L2 *trkin* edits were identified using the same primers (trkin_EX3 and trkin_EX4), while Ab10 *trkin2* was detected using a separate pair of primers (Ptrkin_EX3 and Ptrkin_EX4) (Supplementary Table 6). The thermocycler was preheated to 95°C prior to all PCR reactions. Edits were confirmed by purifying the PCR reaction via Omega Bio-Tek Mag-Bind RxnPure Plus beads (M1386-01) using a 1:1 ratio and Sanger sequencing by Eton Biosciences. The competition assay plants were genotyped using primers specific to an indel in an intron of the *Trkin* gene on K10L2 (Supplementary Table 6). All lines were checked for Cas9 using specific primers (Supplementary Table 6). All reactions were conducted with slightly different temperature profiles and concentrations detailed in Supplementary Table 6.

Immunofluorescence and FISH

Both Immunofluorescence and FISH were performed as described previously (Swentowsky et al. 2020).

Competition assay

To assess the effect of *Trkin* on the ability of K10L2 to suppress Ab10 drive, Ab10 was marked by a dominant functional allele of the *colored 1* (*R1*), and K10L2 was marked by a recessive mutant allele (*r1*). We crossed these plants as the female to an *r1/r1* male and scored segregation of the R1 allele. All experiments were conducted in the UGA Botany greenhouse (Athens, GA, USA) across 4 seasons. In the case of K10L2 *trkin*(–) in 1 season of the experiment, Cas9 was segregating making it impossible to determine what *trkin* mutation was present. However, all plants were derived from an individual with a *trkin* null mutation making it extremely likely that all plants, even those carrying Cas9, were *trkin* null. These are indicated in Supplementary Fig. 9. The crosses from seasons 1 and 2 were in the same genetic background while seasons 3 and 4 involved different genetic backgrounds. Results were analyzed using a Wilcoxon signed-rank test. Plots were generated using R v4.3.1.

Assessment of Ab10 heterozygous drive and fitness

To determine the effect of *Trkin* on Ab10 drive, we generated plants heterozygous for Ab10 and N10 with various *Trkin* genotypes in the same genetic background. Friendly Isles Growing planted all plants in Molokai Hawaii in randomized rows of 15 plants with every other row being an *r1/r1* male. No border corn was used, but edge effects were included in the final statistical model. All Ab10 bearing plants were detasseled and allowed to open pollinate with the *r1/r1* males. Upon completion of the growing season, Friendly Isles Growing harvested all female plants and sent them to the University of Georgia for processing. All ears were scored for defective kernels, a proxy for aborted kernels, defined as clearly defective kernels surrounded by otherwise healthy kernels with no other explanation. These criteria were selected to exclude insect damage, vivipary, and kernel loss during shipment. We shelled the ears and sorted them by color (dark pigmented *R1* and yellow *r1*). The seeds in each packet were counted using an International Marketing and Design Corp. Programmable Packeting Model 900-2 seed counter with the fast set to 7.2 and the slow set to 0.

The meiotic drive data were found to violate the criteria for an ANOVA, so we square root transformed the data to improve its fit, which did not fully satisfy the statistical assumptions for a linear relationship, skew, and kurtosis, but came reasonably close. We chose to proceed with the ANOVA as the residuals appeared normally distributed and alternative statistical methods did not make it possible to account for the necessary number of variables. We included the following covariates in the model: field *x* coordinate, field *y* coordinate, edge of field, and individual who sorted the kernels. The kernel abortion data were very far from a normal distribution so a Kruskal–Wallis test was used. The total kernel number data were analyzed using an ANOVA and met all assumptions. We included the following covariates in the model: field *x* coordinate, field *y* coordinate, edge of field, and individual who sorted the kernels.

Assessment of Ab10 homozygous fitness

To assess the effect of *Trkin* on Ab10 fitness, we created an F2 mapping population segregating for Ab10 *Trkin1*(+) *trkin2*(–) and Ab10 *trkin1*(–) *trkin2*(–). We grew 39 F2 plants and scored

them for their *Trkin1* genotype. We used a χ^2 test to check for deviation from a Mendelian segregation pattern. Plants were placed in a randomized order and grown to maturity in the UGA Botany greenhouse. They were allowed to open pollinate among themselves. We measured plant height and average kernel weight as proxies for plant fitness. We also scored total kernel count, but the experiment was underpowered to detect an effect of any magnitude. All data were analyzed using an ANOVA. Plots were generated using R v4.3.1.

Effect of *Trkin* on male meiotic errors

We scored Ab10 homozygous plants with different *Trkin* genotypes for meiotic errors using the slides prepared for FISH as described above. A meiotic error was defined as a micronucleus in a dyad or tetrad or a microcyte in a dyad or tetrad (Supplementary Fig. 11). Counts of meiotic errors were normalized against the total count of same stage cells observed. Results were analyzed using an ANOVA. Plots were generated using R v4.3.1.

Effect of *Trkin* on unlinked mixed knob

A line carrying a marker gene expressing GFP from a zein promoter (Li *et al.* 2013) that is closely linked to the knob on chromosome 4L (tdsgR106F01) was obtained from the Maize Genetics Cooperation Stock Center, Urbana, IL, USA. We generated lines heterozygous for Ab10 or K10L2 with various *Trkin* genotypes where the GFP insertion was linked to the knob and the opposite chromosome 4L was from the inbred Ms71, which lacks a knob on 4L (Albert *et al.* 2010). Ms71 was obtained as PI 587137 from the Germplasm Resources Information Network, Ames, IA, USA. Cas9 was segregating in the families used for these experiments so it was not possible to determine the exact allele used. However, all plants were derived from an individual with a *trkin* null mutation making it extremely likely that all plants, even those carrying Cas9, were *trkin* null. We then crossed these lines as the female to Ms71 and scored the resulting kernels for GFP fluorescence under visible blue light using a Dark Reader Hand Lamp and Dark Reader Glasses (Clare Chemical Research #HL34T). All data were analyzed using an ANOVA. Plots were generated using R v4.3.1.

Modeling the effect of *trkin* on Ab10 population dynamics

We model the system as a single locus where 4 alleles [Ab10 *Trkin*(+), Ab10 *trkin*(−), K10L2, and N10] are segregating. We initially assumed finite population sizes, discrete nonoverlapping generations, diploid organisms, a single panmictic population, and that all individuals have the same number of offspring. We introduced stochasticity later. We assumed the N10/N10 homozygote is the wild-type genotype and has maximal fitness. We assumed that all heterozygotes experience drive during ovule production; pollen production follows Mendelian transmission and Ab10 *Trkin*(+), Ab10 *trkin*(−), and K10L2 alleles bear a fitness cost (Tables 1 and 2). Ab10 drives against N10 (drive strength: d_1) and K10L2 (drive strength: d_3). K10L2 drives against N10 (drive strength: d_2). The *Trkin*(+) allele suppresses Ab10 drive by an amount of δ_1 ($0 < \delta_1 < d_1$).

Let p_m^+, p_f^+, p_m^-, p_f^-, q_m, and q_f denote the frequencies of the Ab10 *Trkin*(+), Ab10 *trkin*(−), and K10L2 alleles in pollen and ovules respectively in 1 generation. Then, the frequencies of the alleles in the next generation can be given by

$$p_m^{+'} = \frac{1}{\bar{W}}\Big((1-a)p_f^+p_m^+ + \frac{1}{2}(1-a)(p_f^+p_m^- + p_f^-p_m^+) + \frac{1}{2}(1-a\ h_a)(p_m^+(1-p_f^- - p_f^+ - q_f) + p_f^+(1-p_m^- - p_m^+ - q_m)) + \frac{1}{2}(1-a\,h_a)(1-k\,h_k)(p_m^+q_f + p_f^+q_m)\Big), \quad (1)$$

$$p_f^{+'} = \frac{1}{\bar{W}}\Big((1-a)p_f^+p_m^+ + \frac{1}{2}(1-a)(p_f^+p_m^- + p_f^-p_m^+) + \frac{1}{2}(1+d_3)(1-a\,h_a)(1-k\,h_k)(p_m^+q_f + p_f^+q_m) + \frac{1}{2}(1-a\,h_a)(p_m^+(1-p_f^- - p_f^+ - q_f) + p_f^+(1-p_m^- - p_m^+ - q_m))(1+d_1-\delta_1)\Big), \quad (2)$$

$$p_m^{-'} = \frac{1}{\bar{W}}\Big((1-a)p_f^-p_m^- + \frac{1}{2}(1-a)(p_f^+p_m^- - + p_f^-p_m^+) + \frac{1}{2}(1-a\,h_a)(p_m^-(1-p_f^- - p_f^+ - q_f) + p_f^-(1-p_m^- - p_m^+ - q_m)) + \frac{1}{2}(1-a\,h_a)(1-k\,h_k)(p_m^-q_f + p_f^-q_m)\Big), \quad (3)$$

$$p_f^{-'} = \frac{1}{\bar{W}}\Big((1-a)p_f^-p_m^- + \frac{1}{2}(1-a)(p_f^+p_m^- + p_f^-p_m^+) + \frac{1}{2}(1+d_1)(1-a\,h_a)(p_m^-(1-p_f^- - p_f^+ - q_f) + p_f^-(1-p_m^- - p_m^+ - q_m)) + \frac{1}{2}(1+d_3)(1-a\,h_a)(1-k\,h_k)(p_m^-q_f + p_f^-q_m)\Big), \quad (4)$$

$$q_m' = \frac{1}{\bar{W}}\Big((1-k)q_fq_m + \frac{1}{2}(1-a\,h_a)(1-k\,h_k)(p_m^-q_f + p_f^-q_m) + \frac{1}{2}(1-a\,h_a)(1-k\,h_k)(p_m^+q_f + p_f^+q_m) + \frac{1}{2}(1-k\,h_k)(q_f(1-p_m^- - p_m^+ - q_m) + (1-p_f^- - p_m^+ - q_f)q_m)\Big), \quad (5)$$

$$q_f' = \frac{1}{\bar{W}}\Big((1-k)q_fq_m + \frac{1}{2}(1-d_3)(1-a\,h_a)(1-k\,h_k)(p_m^-q_f + p_f^-q_m) + \frac{1}{2}(1-d_3)(1-a\,h_a)(1-k\,h_k)(p_m^+q_f + p_f^+q_m) + \frac{1}{2}(1+d_2)(1-k\,h_k)(q_f(1-p_m^- - p_m^+ - q_m) + (1-p_f^- - p_f^+ - q_f)q_m)\Big). \quad (6)$$

Here, the mean fitness $\bar{W}$ can be calculated using

$$\bar{W} = (1-a)p_f^-p_m^- + (1-a)p_f^+p_m^+ + (1-a)(p_f^+p_m^- + p_f^-p_m^+) + (1-a\,h_a)(p_m^-(1-p_f^- - p_f^+ - q_f) + p_f^-(1-p_m^- - p_m^+ - q_m)) + (1-a\,h_a)(p_m^+(1-p_f^- - p_f^+ - q_f) + p_f^+(1-p_m^- - p_m^+ - q_m)) + (1-p_f^- - p_f^+ - q_f)(1-p_m^- - p_m^+ - q_m) + (1-k)q_fq_m + (1-a\,h_a)(1-k\,h_k)(p_m^-q_f + p_f^-q_m) + (1-a\,h_a)(1-k\,h_k)(p_m^+q_f + p_f^+q_m) + (1-k\,h_k)(q_f(1-p_m^- - p_m^+ - q_m) + (1-p_f^- - p_f^+ - q_f)q_m). \quad (7)$$

The frequency of N10 allele in pollen and ovules can be calculated using $(1-p_m^- - p_m^+ - q_m)$ and $(1-p_f^- - p_f^+ - q_f)$, respectively. We track the frequencies separately in the 2 sexes such that the frequencies in males and females each add up to 1, and the population always has equal sex ratios.

Table 1. Fitness and proportion of ovules and pollen produced by each genotype.

	Proportion ovules				Proportion pollen				
Genotype	**N10**	**Ab10^{trkin+}**	**Ab10^{trkin-}**	**K10**	**N10**	**Ab10^{trkin+}**	**Ab10^{trkin-}**	**K10**	**Fitness**
N10/N10	1				1				1
N10/Ab10^{trkin-}	$(1-d_1)/2$		$(1+d_1)/2$		1/2		1/2		$1-h_a a$
N10/Ab10^{trkin+}	$(1-d_1+\delta_1)/2$	$(1+d_1-\delta_1)/2$			1/2	1/2			$1-h_a a$
N10/K10	$(1-d_2)/2$			$(1+d_2)/2$	1/2			1/2	$1-h_k k$
Ab10^{trkin-}/Ab10^{trkin-}			1				1		$1-a$
Ab10^{trkin+}/Ab10^{trkin-}		1/2	1/2			1/2	1/2		$1-a$
Ab10^{trkin+}/Ab10^{trkin+}			1				1		$1-a$
K10/K10				1				1	$1-k$
K10/Ab10^{trkin+}	$(1-d_3)/2$	$(1+d_3)/2$			1/2	1/2			$(1-h_a a)*(1-h_k k)$
K10/Ab10^{trkin-}	$(1-d_3)/2$		$(1+d_3)/2$		1/2		1/2		$(1-h_a a)*(1-h_k k)$

Table 2. Ab10 *Trkin* model parameters.

Variable/parameter	Description
d_1	Drive strength of Ab10 against N10
δ_1	Amount of Ab10 drive suppressed by *Trkin*(+)
d_2	Drive strength of K10L2 against N10
d_3	Drive strength of Ab10 against K10L2
a	Fitness cost of Ab10 homozygote
h_a	Dominance coefficient for Ab10/N10
k	Fitness cost of K10L2 homozygote
h_k	Dominance coefficient for K10L2/N10

All parameters range between 0 and 1 except δ_1, which ranges between 0 and d_1.

We use a subset of parameters for the simulations based on empirical observations from the maize system—$h_a = 0.25$, $h_k = 0.2$, $a = 0.6$, $k = 0.225$, $d_1 = 0.4$ (drive strength of Ab10 against N10 = 70%), $d_2 = 0.1$ (drive strength of K10L2 against N10 = 55%), and $d_3 = 0.1$ (drive strength of Ab10 against K10L2 = 55%) (Kanizay *et al.* 2013; Higgins *et al.* 2018).

At this parameter subset, at $\delta_1 = 0$, at equilibrium, both Ab10 and K10L2 persist at a frequency of 5% each and the frequencies of Ab10 *Trkin*(+) and Ab10 *trkin*(–) are equal (deterministically).

Testing the range of d_1 where Ab10 *Trkin*(+) and Ab10 *trkin*(–) can invade a population

We ran these simulations deterministically for a range of δ_1 ($0 < \delta_1 < 0.4$) using an effective population size, N_e of 10,000 (Tittes *et al.* 2025) for 5,000 generations (sufficient to reach equilibrium) with initial frequencies of Ab10 *Trkin*(+) and K10L2 at 5%, and Ab10 *trkin*(–) at $1/N_e$ (equal frequencies in both sexes). At any $\delta_1 > 0$, Ab10 *trkin*(–) always invades the population and replaces Ab10 *Trkin*(+).

We also tested for the invasion of Ab10 *Trkin*(+) similarly by starting the simulations with initial frequencies of Ab10 *trkin*(–) and K10L2 at 5% and Ab10 *Trkin*(+) at $1/N_e$ (equal frequencies in both sexes). For any value δ_1, Ab10 *Trkin*(+) could never invade the population.

This suggests that the selection against Ab10 *Trkin*(+) is strong enough to prevent its invasion in a population containing Ab10 *trkin*(–) and Ab10 *trkin*(–) can invade a population containing Ab10 *Trkin*(+) and replace it (Fig. 10a and b).

Testing the strength of selection for a range of d_1 and calculating the selection coefficients such that $2 N_e s < 1$ (nearly neutral zone)

For the calculation of the relative selective benefit (s) for Ab10 *trkin*(–), we ran the simulations for a range of δ_1 ($0 < \delta_1 < 0.4$) for 5,000 generations (sufficient to reach equilibrium) with initial frequencies of Ab10 *Trkin*(+) and K10L2 at $1/N_e$ and Ab10 *trkin*(–) at 0. Then, after 5,000 generations, we introduced Ab10 *trkin*(–) at a frequency of $1/N_e$ (only in females) into the population at equilibrium. Then, we ran the simulation for 1 more generation and calculated the relative selective benefit of Ab10 *trkin*(–), s using allele frequencies after generation 5,000 using

$$s = \left(\frac{p_m^{-\prime} + p_f^{-\prime}}{p_m^{-} + p_f^{-}} \Big/ \frac{p_m^{+\prime} + p_f^{+\prime}}{p_m^{+} + p_f^{+}} \right) - 1. \quad (8)$$

This "s" was used to calculate the 2 $N_e s$ parameter for a range of values of N_e ($10^2 < N_e < 10^4$) and δ_1 ($0 < \delta_1 < 0.4$). We found that $2 N_e s < 1$ only for a very small subset where $d_1 < 0.01$ and $N_e \sim 100$ (the approximate value of δ_1 from empirical observations in the maize system should be ~0.1) (Fig. 9a). This suggests that selection against Ab10 *Trkin*(+) is strong and it could not be maintained in the population by drift (since $2 N_e s >> 1$). This would imply that Ab10 *Trkin*(+) could not persist in the population in the presence of Ab10 *trkin*(–). Ab10 *Trkin*(+) is probably older than Ab10 *trkin*(–) and could be in the process of being replaced from the populations by invasion from Ab10 *trkin*(–).

Testing how long Ab10 *Trkin*(+) can persist in a population that is being invaded by Ab10 *trkin*(–)

We ran these simulations stochastically (modeling drift following a multinomial distribution) at $N_e = 10{,}000$ and for a range of δ_1 ($0 < \delta_1 < 0.4$) (Tittes *et al.* 2025). We started our populations at an initial frequency of 6% for Ab10 *Trkin*(+) and K10L2 and $1/N_e$ for Ab10 *trkin*(–) (equal frequencies in both sexes). For each parameter value, each simulation was run 10,000 times, as Ab10 *trkin*(–) was often lost due to drift.

For the subset of simulations where Ab10 *trkin*(–) could successfully invade and replace Ab10 *Trkin*(+), we looked at the time taken for loss of Ab10 *Trkin*(+) from the population. For most values of δ_1, Ab10 *Trkin*(+) was lost within 500 generations. From empirical estimates, $\delta_1 \sim 0.1$, thus, Ab10 *Trkin*(+) would be expected to persist for ~200 generations (Fig. 10d).

We also looked at the proportion of times Ab10 *trkin*(–) (escaping stochastic loss due to drift) could successfully invade the population and outcompete Ab10 *Trkin*(+) (Fig. 10a). This proportion was small, and for $\delta_1 \sim 0.1$, about 2.5% of the times Ab10 *trkin*(–) could escape stochastic loss and outcompete Ab10 *Trkin*(+).

Data availability

All codes, the Ab10 and K10L2 haplotype assemblies and genome annotations, and plasmid information are available at

https://github.com/dawelab/TRKIN_Published.git. Raw PacBio HiFi data for Ab10 and CI66 are available on the NCBI SRA under BioProject PRJNA1254310.

Supplemental material available at GENETICS online.

Acknowledgments

We thank Dr. Jianing Liu for her assistance in the B73-Ab10 v2 assembly. We thank Tanvi Kamat and Anne Blevins for sorting and counting kernels. We thank Dr. Zenglu Li and lab for generously allowing us to use their seed counter. We also thank the USDA-ARS Germplasm Resources Information Network and Maize Genetics Cooperation Stock Center for supplying seed stocks, as well as the Georgia Advanced Computing Resource Center for their technical support.

Funding

This work was supported by an National Institutes of Health training grant (T32GM007103) and National Science Foundation (NSF) fellowship to MJB (2236869), an NSF grant to RLU (204705), and an NSF grant to RKD (1925546).

Conflicts of interest

The authors declare no conflicts of interest.

Literature cited

Albert PS, Gao Z, Danilova TV, Birchler JA. 2010. Diversity of chromosomal karyotypes in maize and its relatives. Cytogenet Genome Res. 129(1-3):6–16. doi:10.1159/000314342.

Alexa A, Rahnenfuhrer J. 2024. topGO: enrichment analysis for gene ontology. doi:10.18129/B9.bioc.topGO.

Alonge M, Lebeigle L, Kirsche M, Jenike K, Ou S, Aganezov S, Wang X, Lippman ZB, Schatz MC, Soyk S. 2022. Automated assembly scaffolding using RagTag elevates a new tomato system for high-throughput genome editing. Genome Biol. 23(1):258. doi:10.1186/s13059-022-02823-7.

Barnett DW, Garrison EK, Quinlan AR, Strömberg MP, Marth GT. 2011. BamTools: a C++ API and toolkit for analyzing and managing BAM files. Bioinformatics. 27(12):1691–1692. doi:10.1093/bioinformatics/btr174.

Bolger AM, Lohse M, Usadel B. 2014. Trimmomatic: a flexible trimmer for Illumina sequence data. Bioinformatics. 30(15):2114–2120. doi:10.1093/bioinformatics/btu170.

Brady MJ, Cheam M, Gent JI, Dawe RK. 2024. The maize striate leaves2 (sr2) gene encodes a conserved DUF3732 domain and is homologous to the rice yss1 gene. Plant Direct. 8(2):e567. doi:10.1002/pld3.567.

Bravo Núñez MA, Lange JJ, Zanders SE. 2018. A suppressor of a wtf poison-antidote meiotic driver acts via mimicry of the driver's antidote. PLoS Genet. 14(11):e1007836. doi:10.1371/journal.pgen.1007836.

Buckler ES IV, Phelps-Durr TL, Buckler CS, Dawe RK, Doebley JF, Holtsford TP. 1999. Meiotic drive of chromosomal knobs reshaped the maize genome. Genetics. 153(1):415–426. doi:10.1093/genetics/153.1.415.

Burt A, Trivers R. 2008. Genes in Conflict the Biology of Selfish Genetic Elements. Cambridge, London, England (MA): Harvard University Press.

Camacho C, Boratyn GM, Joukov V, Vera Alvarez R, Madden TL. 2023. ElasticBLAST: accelerating sequence search via cloud computing. BMC Bioinformatics. 24(1):117. doi:10.1186/s12859-023-05245-9.

Cheng H, Concepcion GT, Feng X, Zhang H, Li H. 2021. Haplotype-resolved de novo assembly using phased assembly graphs with hifiasm. Nat Methods. 18(2):170–175. doi:10.1038/s41592-020-01056-5.

Clark FE, Akera T. 2021. Unravelling the mystery of female meiotic drive: where we are. Open Biol. 11(9):210074. doi:10.1098/rsob.210074.

Clarke JD. 2009. Cetyltrimethyl ammonium bromide (CTAB) DNA miniprep for plant DNA isolation. Cold Spring Harb Protoc. 2009(3):pdb.prot5177. doi:10.1101/pdb.prot5177.

Danecek P, Bonfield JK, Liddle J, Marshall J, Ohan V, Pollard MO, Whitwham A, Keane T, McCarthy SA, Davies RM, *et al.* 2021. Twelve years of SAMtools and BCFtools. Gigascience. 10(2):giab008. doi:10.1093/gigascience/giab008.

Dawe RK. 2022. The maize abnormal chromosome 10 meiotic drive haplotype: a review. Chromosome Res. 30(2-3):205–216. doi:10.1007/s10577-022-09693-6.

Dawe RK, Lowry EG, Gent JI, Stitzer MC, Swentowsky KW, Higgins DM, Ross-Ibarra J, Wallace JG, Kanizay LB, Alabady M, *et al.* 2018. A Kinesin-14 motor activates neocentromeres to promote meiotic drive in maize. Cell. 173(4):839–850.e18. doi:10.1016/j.cell.2018.03.009.

Doyle JJ, Doyle JL. 1987. A rapid DNA isolation procedure from small quantities of fresh leaf tissues. Phytochem Bull. 19:11–15.

Emms DM, Kelly S. 2019. OrthoFinder: phylogenetic orthology inference for comparative genomics. Genome Biol. 20(1):238. doi:10.1186/s13059-019-1832-y.

Fishman L, Kelly JK. 2015. Centromere-associated meiotic drive and female fitness variation in *Mimulus*. Evolution. 69(5):1208–1218. doi:10.1111/evo.12661.

Gabler F, Nam S-Z, Till S, Mirdita M, Steinegger M, Söding J, Lupas AN, Alva V. 2020. Protein sequence analysis using the MPI bioinformatics toolkit. Curr Protoc Bioinformatics. 72(1):e108. doi:10.1002/cpbi.108.

Gabriel L, Brůna T, Hoff KJ, Ebel M, Lomsadze A, Borodovsky M, Stanke M. 2024. BRAKER3: Fully automated genome annotation using RNA-seq and protein evidence with GeneMark-ETP, AUGUSTUS, and TSEBRA. Genome Res. 34(5):769–777. https://doi.org/10.1101/gr.278090.123.

Haas BJ, Delcher AL, Mount SM, Wortman JR, Smith RK Jr, Hannick LI, Maiti R, Ronning CM, Rusch DB, Town CD, *et al.* 2003. Improving the Arabidopsis genome annotation using maximal transcript alignment assemblies. Nucleic Acids Res. 31(19):5654–5666. doi:10.1093/nar/gkg770.

Haas BJ, Papanicolaou A, Yassour M, Grabherr M, Blood PD, Bowden J, Couger MB, Eccles D, Li B, Lieber M, *et al.* 2013. De novo transcript sequence reconstruction from RNA-seq using the Trinity platform for reference generation and analysis. Nat Protoc. 8(8):1494–1512. doi:10.1038/nprot.2013.084.

Haig D, Grafen A. 1991. Genetic scrambling as a defence against meiotic drive. J Theor Biol. 153(4):531–558. doi:10.1016/S0022-5193(05)80155-9.

Haldane JBS. 1927. A mathematical theory of natural and artificial selection, part V: selection and mutation. Math Proc Camb Philos Soc. 23(7):838–844. doi:10.1017/S0305004100015644.

Hall DW, Dawe RK. 2018. Modeling the evolution of female meiotic drive in maize. G3 (Bethesda). 8(1):123–130. doi:10.1534/g3.117.300073.

Hart AJ, Ginzburg S, Xu MS, Fisher CR, Rahmatpour N, Mitton JB, Paul R, Wegrzyn JL. 2020. EnTAP: bringing faster and smarter

functional annotation to non-model eukaryotic transcriptomes. Mol Ecol Resour. 20(2):591–604. doi:10.1111/1755-0998.13106.
Hartl DL. 1970. Analysis of a general population genetic model of meiotic drive. Evolution. 24(3):538. doi:10.2307/2406834.
Hartl DL, Clark AG. 2007. Principles of Population Genetics. New York (NY): Oxford University Press.
Hiatt EN, Dawe RK. 2003. Four loci on abnormal chromosome 10 contribute to meiotic drive in maize. Genetics. 164(2):699–709. doi:10.1093/genetics/164.2.699.
Hiatt EN, Kentner EK, Dawe RK. 2002. Independently regulated neocentromere activity of two classes of tandem repeat arrays. Plant Cell. 14(2):407–420. doi:10.1105/tpc.010373.
Higgins DM, Lowry EG, Kanizay LB, Becraft PW, Hall DW, Dawe RK. 2018. Fitness costs and variation in transmission distortion associated with the abnormal chromosome 10 meiotic drive system in maize. Genetics. 208(1):297–305. doi:10.1534/genetics.117.300060.
Higgins DM, Nannas NJ, Dawe RK. 2016. The maize divergent spindle-1 (dv1) gene encodes a Kinesin-14A motor protein required for meiotic spindle pole organization. Front Plant Sci. 7:1277. doi:10.3389/fpls.2016.01277.
Hon T, Mars K, Young G, Tsai Y-C, Karalius JW, Landolin JM, Maurer N, Kudrna D, Hardigan MA, Steiner CC, *et al.* 2020. Highly accurate long-read HiFi sequencing data for five complex genomes. Sci Data. 7(1):399. doi:10.1038/s41597-020-00743-4.
Dainat J. 2020. AGAT: another Gff Analysis Toolkit to handle annotations in any GTF/GFF format. Zenodo. https://www.doi.org/10.5281/zenodo.3552717
Hufford MB, Seetharam AS, Woodhouse MR, Chougule KM, Ou S, Liu J, Ricci WA, Guo T, Olson A, Qiu Y, *et al.* 2021. De novo assembly, annotation, and comparative analysis of 26 diverse maize genomes. Science. 373(6555):655–662. doi:10.1126/science.abg5289.
Kanizay LB, Albert PS, Birchler JA, Dawe RK. 2013. Intragenomic conflict between the two major knob repeats of maize. Genetics. 194(1):81–89. doi:10.1534/genetics.112.148882.
Kato YTA. 1976. Cytological studies of maize (*Zea mays* L.) and teosinte (*Zea mexicana* Schrader Kuntze) in relation to their origin and evolution. Mass Agric Exp Stn Bull. 635:1–185. doi:10.7275/20482802.
Kim D, Paggi JM, Park C, Bennett C, Salzberg SL. 2019. Graph-based genome alignment and genotyping with HISAT2 and HISAT-genotype. Nat Biotechnol. 37(8):907–915. doi:10.1038/s41587-019-0201-4.
Kosugi S, Hasebe M, Tomita M, Yanagawa H. 2009. Systematic identification of cell cycle-dependent yeast nucleocytoplasmic shuttling proteins by prediction of composite motifs. Proc Natl Acad Sci U S A. 106(25):10171–10176. doi:10.1073/pnas.0900604106.
Kuznetsov D, Tegenfeldt F, Manni M, Seppey M, Berkeley M, Kriventseva EV, Zdobnov EM. 2023. OrthoDB v11: annotation of orthologs in the widest sampling of organismal diversity. Nucleic Acids Res. 51(D1):D445–D451. doi:10.1093/nar/gkac998.
Labun K, Montague TG, Krause M, Torres Cleuren YN, Tjeldnes H, Valen E. 2019. CHOPCHOP v3: expanding the CRISPR web toolbox beyond genome editing. Nucleic Acids Res. 47(W1):W171–W174. doi:10.1093/nar/gkz365.
Lampson MA, Black BE. 2017. Cellular and molecular mechanisms of centromere drive. Cold Spring Harb Symp Quant Biol. 82:249–257. doi:10.1101/sqb.2017.82.034298.
Li Y, Segal G, Wang Q, Dooner HK. 2013. Gene tagging with engineered Ds elements in maize. Methods Mol Biol. 1057:83–99. doi:10.1007/978-1-62703-568-2_6.
Liao Y, Smyth GK, Shi W. 2014. featureCounts: an efficient general purpose program for assigning sequence reads to genomic features. Bioinformatics. 30(7):923–930. doi:10.1093/bioinformatics/btt656.
Lindholm AK, Dyer KA, Firman RC, Fishman L, Forstmeier W, Holman L, Johannesson H, Knief U, Kokko H, Larracuente AM, *et al.* 2016. The ecology and evolutionary dynamics of meiotic drive. Trends Ecol Evol. 31(4):315–326. doi:10.1016/j.tree.2016.02.001.
Liu J, Seetharam AS, Chougule K, Ou S, Swentowsky KW, Gent JI, Llaca V, Woodhouse MR, Manchanda N, Presting GG, *et al.* 2020. Gapless assembly of maize chromosomes using long-read technologies. Genome Biol. 21(1):121. doi:10.1186/s13059-020-02029-9.
Marçais G, Delcher AL, Phillippy AM, Coston R, Salzberg SL, Zimin A. 2018. MUMmer4: a fast and versatile genome alignment system. PLoS Comput Biol. 14(1):e1005944. doi:10.1371/journal.pcbi.1005944.
McDonald HB, Stewart RJ, Goldstein LS. 1990. The Kinesin-like ncd protein of *Drosophila* is a minus end-directed microtubule motor. Cell. 63(6):1159–1165. doi:10.1016/0092-8674(90)90412-8.
O'Leary NA, Wright MW, Brister JR, Ciufo S, Haddad D, McVeigh R, Rajput B, Robbertse B, Smith-White B, Ako-Adjei D, *et al.* 2016. Reference sequence (RefSeq) database at NCBI: current status, taxonomic expansion, and functional annotation. Nucleic Acids Res. 44(D1):D733–D745. doi:10.1093/nar/gkv1189.
Paz MM, Shou H, Guo Z, Zhang Z, Banerjee AK, Wang K. 2004. Assessment of conditions affecting *Agrobacterium*-mediated soybean transformation using the cotyledonary node explant. Euphytica. 136(2):167–179. doi:10.1023/B:EUPH.0000030670.36730.a4.
Pertea M, Pertea GM, Antonescu CM, Chang T-C, Mendell JT, Salzberg SL. 2015. StringTie enables improved reconstruction of a transcriptome from RNA-seq reads. Nat Biotechnol. 33(3):290–295. doi:10.1038/nbt.3122.
Piperno DR, Ranere AJ, Holst I, Iriarte J, Dickau R. 2009. Starch grain and phytolith evidence for early ninth millennium B.P. maize from the Central Balsas River Valley, Mexico. Proc Natl Acad Sci U S A. 106(13):5019–5024. doi:10.1073/pnas.0812525106.
Plačková K, Bureš P, Lysak MA, Zedek F. 2024. Centromere drive may propel the evolution of chromosome and genome size in plants. Ann Bot. 134(6):1067–1076. doi:10.1093/aob/mcae149.
Price TAR, Windbichler N, Unckless RL, Sutter A, Runge J-N, Ross PA, Pomiankowski A, Nuckolls NL, Montchamp-Moreau C, Mideo N, *et al.* 2020. Resistance to natural and synthetic gene drive systems. J Evol Biol. 33(10):1345–1360. doi:10.1111/jeb.13693.
Quinlan AR, Hall IM. 2010. BEDTools: a flexible suite of utilities for comparing genomic features. Bioinformatics. 26(6):841–842. doi:10.1093/bioinformatics/btq033.
Sayers EW, Bolton EE, Brister JR, Canese K, Chan J, Comeau DC, Connor R, Funk K, Kelly C, Kim S, *et al.* 2022. Database resources of the national center for biotechnology information. Nucleic Acids Res. 50(D1):D20–D26. doi:10.1093/nar/gkab1112.
Searle JB, Pardo-Manuel de Villena F. 2024. Meiotic drive and speciation. Annu Rev Genet. 58(1):341–363. doi:10.1146/annurev-genet-111523-102603.
Shumate A, Salzberg SL. 2021. Liftoff: accurate mapping of gene annotations. Bioinformatics. 37(12):1639–1643. doi:10.1093/bioinformatics/btaa1016.
Smit AFA, Hubley R, Green P. RepeatMasker Open-4.0. 2013–2015. [accessed 11 Oct 2024]. http://www.repeatmasker.org.
Svitashev S, Young JK, Schwartz C, Gao H, Falco SC, Cigan AM. 2015. Targeted mutagenesis, precise gene editing, and site-specific gene insertion in maize using Cas9 and guide RNA. Plant Physiol. 169(2):931–945. doi:10.1104/pp.15.00793.

Swentowsky KW, Gent JI, Lowry EG, Schubert V, Ran X, Tseng K-F, Harkess AE, Qiu W, Dawe RK. 2020. Distinct kinesin motors drive two types of maize neocentromeres. Genes Dev. 34(17–18): 1239–1251. doi:10.1101/gad.340679.120.

Thorvaldsdóttir H, Robinson JT, Mesirov JP. 2013. Integrative Genomics Viewer (IGV): high-performance genomics data visualization and exploration. Brief Bioinform. 14(2):178–192. doi:10.1093/bib/bbs017.

Tittes S, Lorant A, McGinty SP, Holland JB, de Jesus Sánchez-González J, Seetharam A, Tenaillon M, Ross-Ibarra J. 2025. The population genetics of convergent adaptation in maize and teosinte is not locally restricted. eLife. 12:RP92405. doi:10.7554/eLife.92405.

UniProt Consortium. 2023. UniProt: the universal protein knowledgebase in 2023. Nucleic Acids Res. 51(D1):D523–D531. doi:10.1093/nar/gkac1052.

Wang J, Chitsaz F, Derbyshire MK, Gonzales NR, Gwadz M, Lu S, Marchler GH, Song JS, Thanki N, Yamashita RA, *et al.* 2023. The conserved domain database in 2023. Nucleic Acids Res. 51(D1): D384–D388. doi:10.1093/nar/gkac1096.

Wang N, Gent JI, Kelly Dawe R. 2021. Haploid induction by a maize cenh3 null mutant. Sci Adv. 7(4):eabe2299. doi:10.1126/sciadv.abe2299.

Yang N, Wang Y, Liu X, Jin M, Vallebueno-Estrada M, alfee E, Chen L, Dilkes BP, Gui S, Fan X, *et al.* 2023. Two teosintes made modern maize. Science. 382(6674):eadg8940. doi:10.1126/science.adg8940.

Editor: D. Barbash